Review of Infrared Properties of GPS and CSS Sources

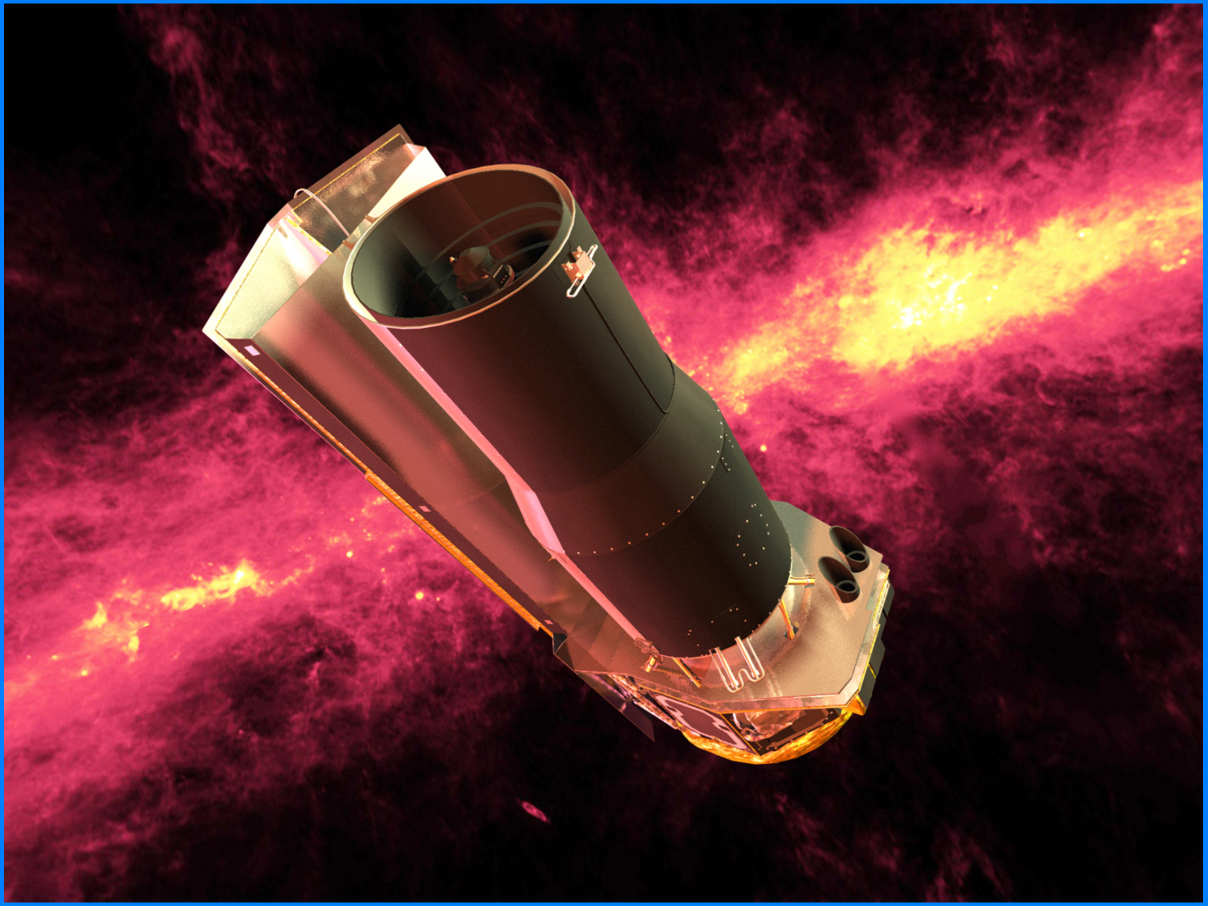

Chris O'Dea *(Univ. of Manitoba, RIT)*

OUTLINE

- Introduction to Infrared Diagnostics
- Large Radio Galaxies (selected topics, for context)
- GPS and CSS Sources
- Implications

Intro to IR Diagnostics

The Parts of an Active Galactic Nucleus

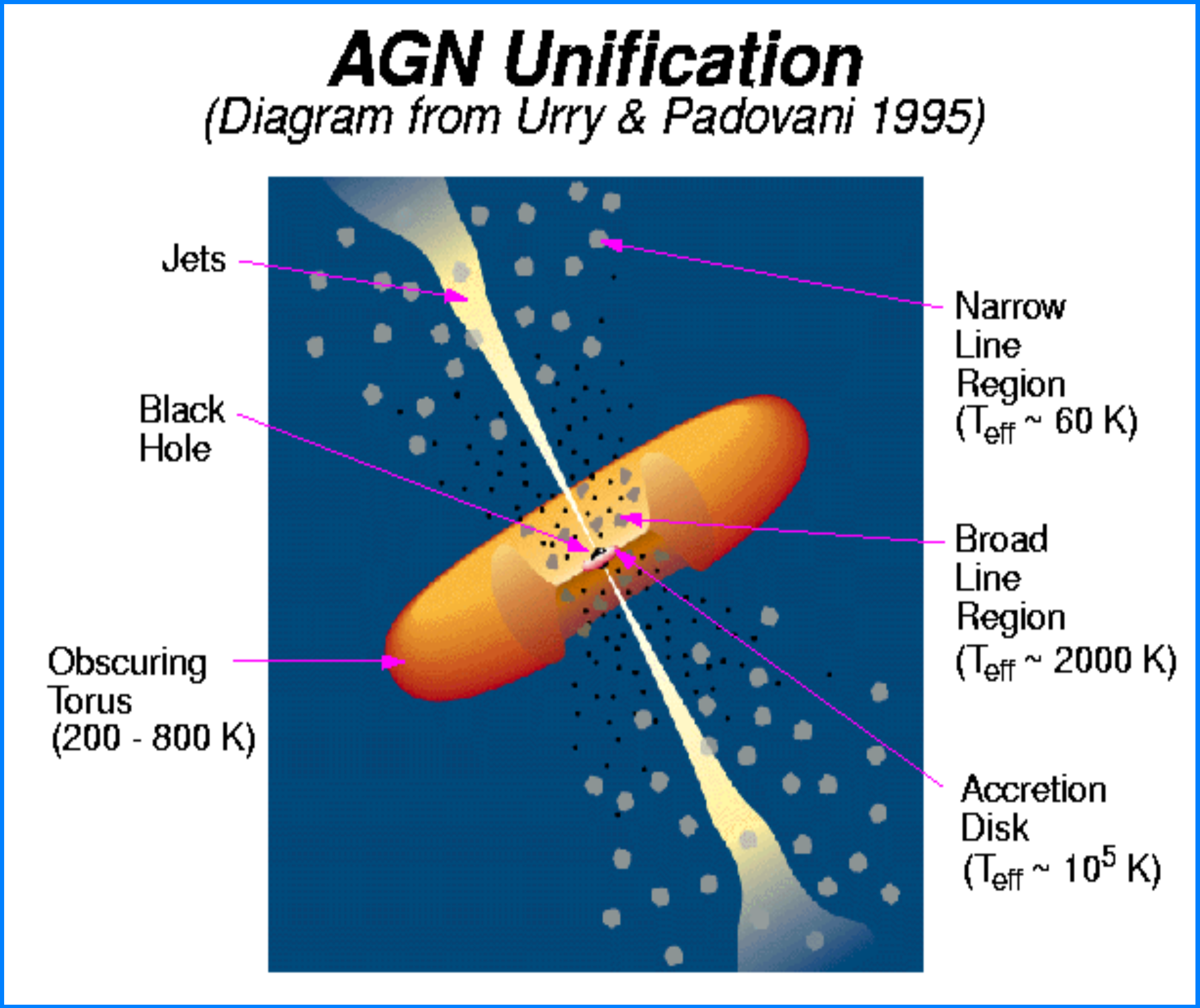

Annotated by M. Voit

Why the Infrared?

- The optical depths Imuch less in IR than optical.
- IRS spectra rich in diagnostic lines/features – dust continuum, PAHs, Fine-structure lines, Sil 9.7 and 18 µm (e.g., Voit 1992, Spinoglio & Malkan 1993, Genzel et al. 1998, Sturm et al. 2002).
- AGN UV-optical light re-radiated in IR by dust in the obscuring material.

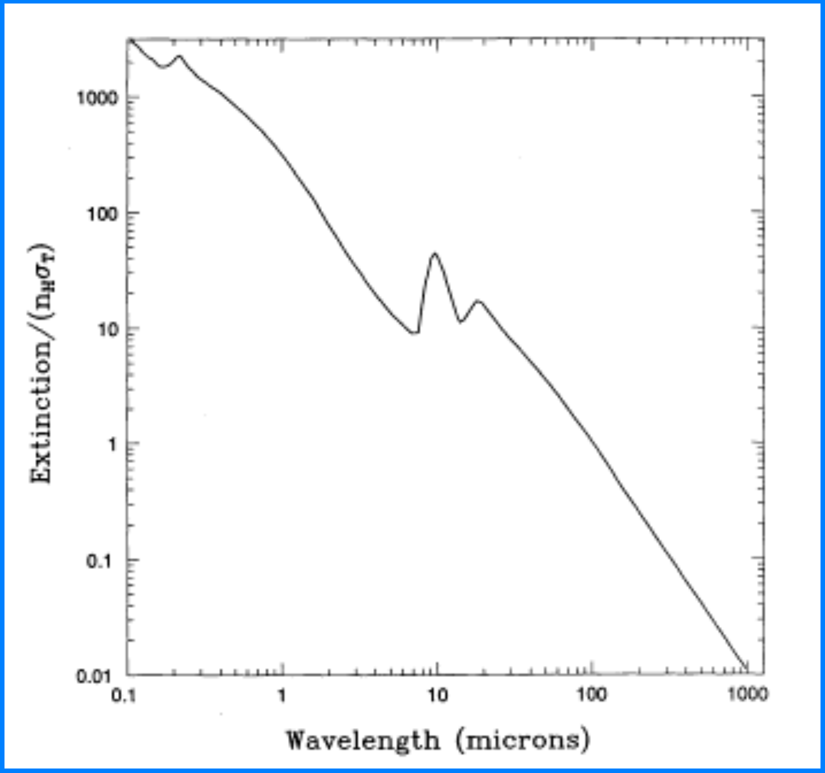

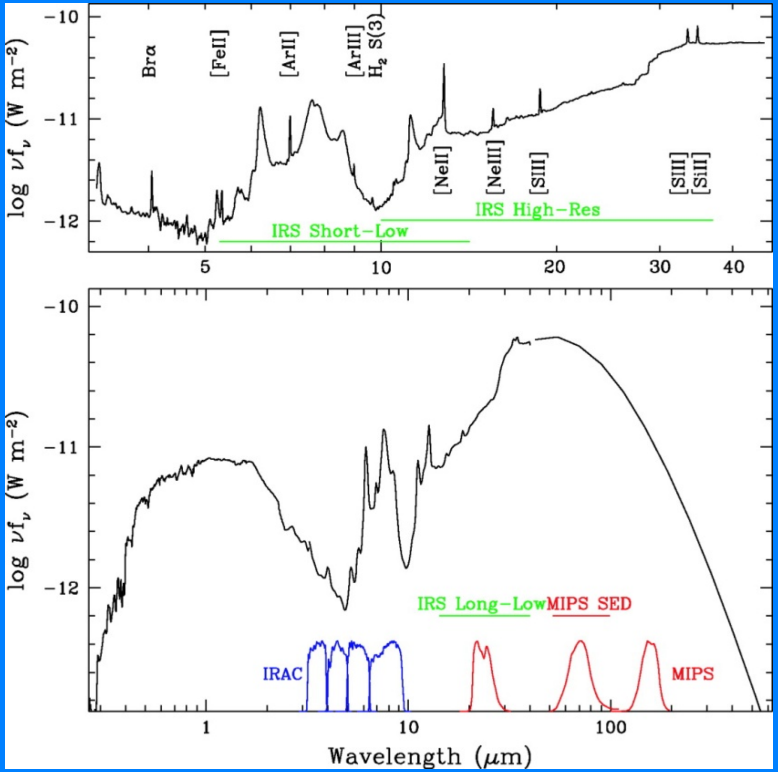

(Top). Dust extinction in units of Thomson optical depth from Draine & Lee (1984) via Pier & Krolik (1992). Note the Silicate features at 9.7 and 18 µm. (Bottom). Schematic spectrum of star forming galaxy showing location of Spitzer bandpasses (Kennicutt et al 2003).

The Planck (Black Body) Function

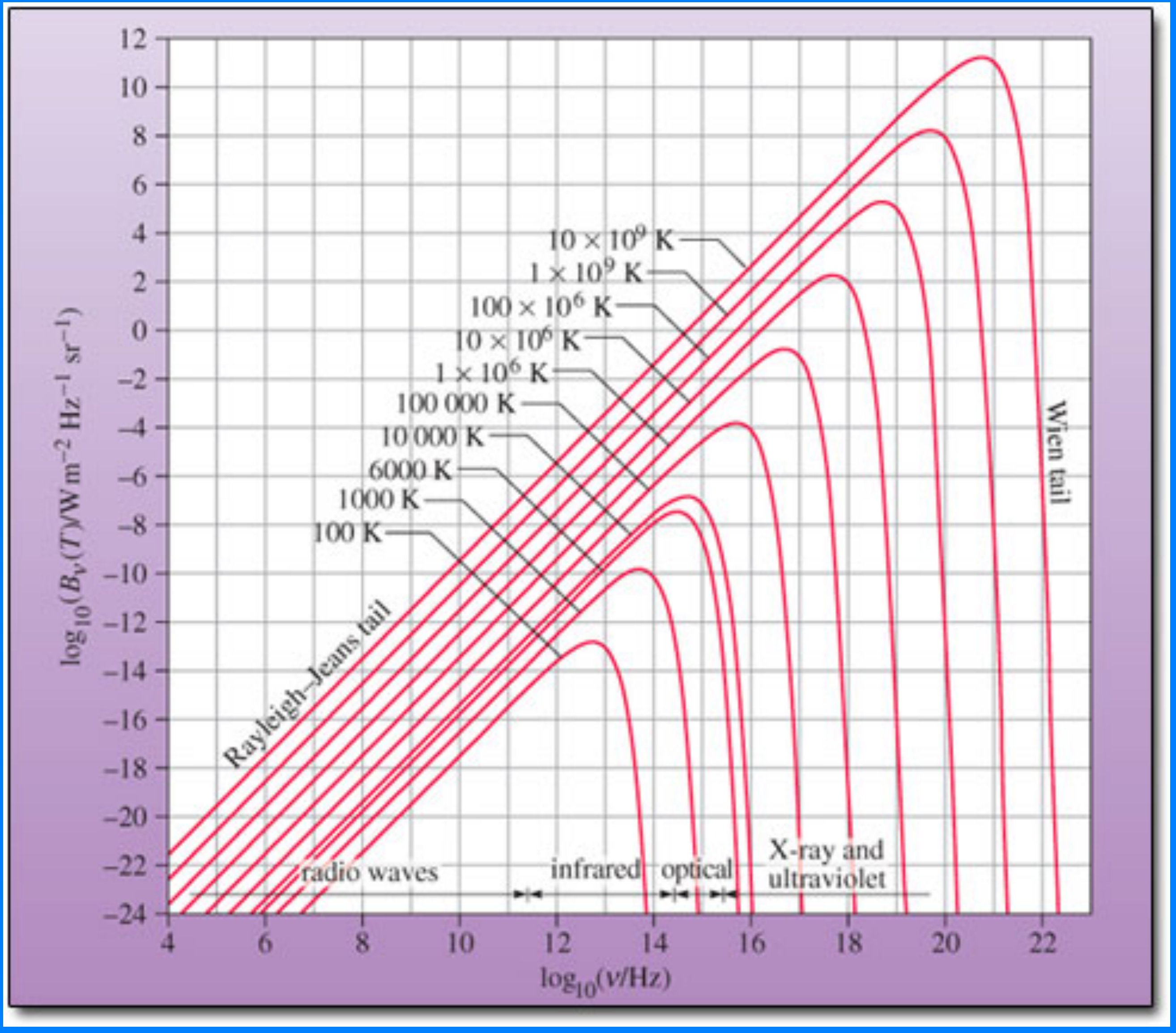

Introduction to Si 9.7 µm Strength

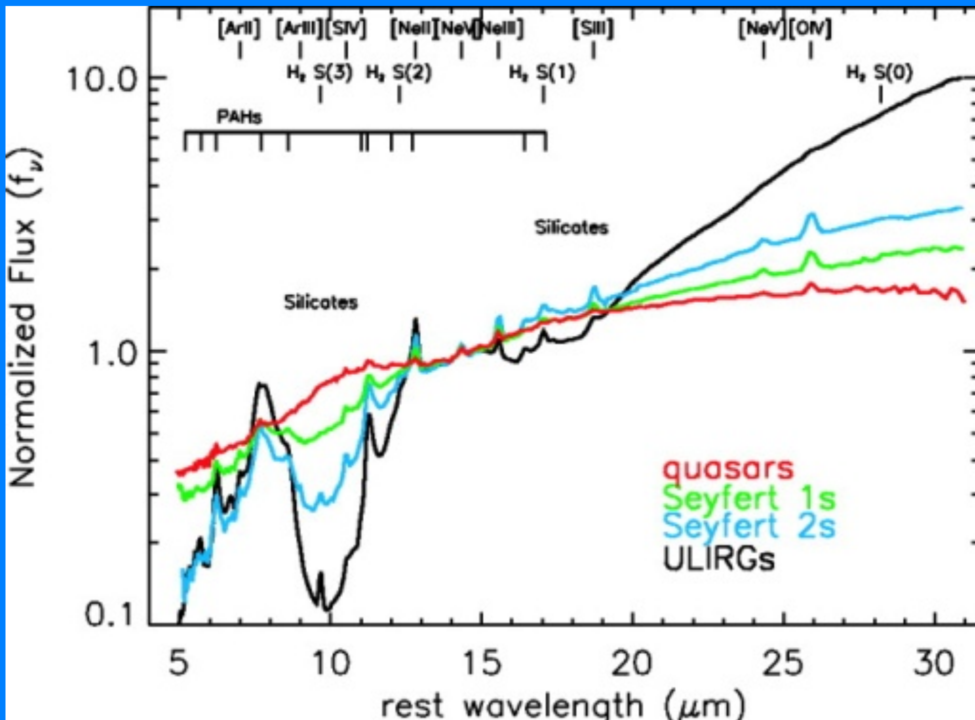

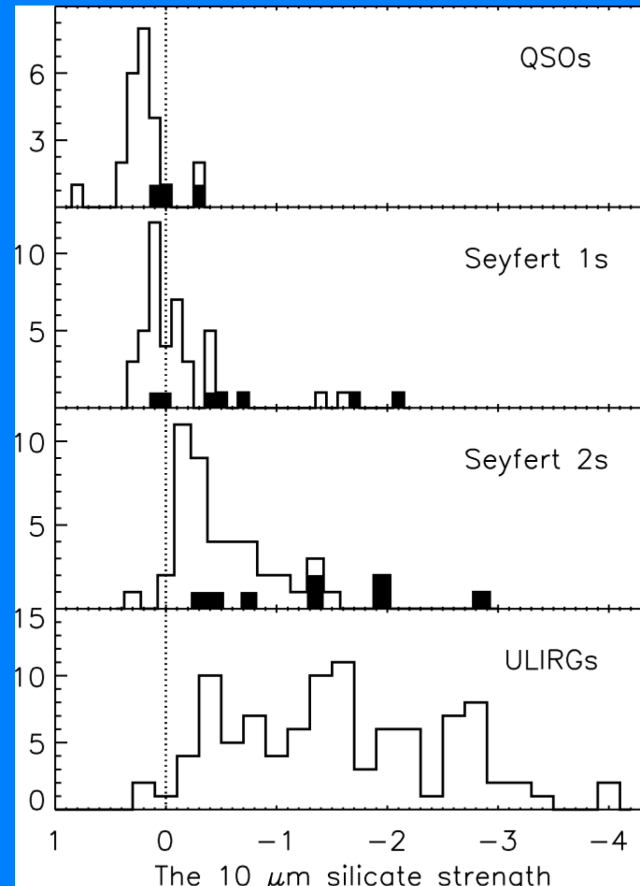

- $S_{9.7} = \ln(F_{9.7}/F_{cont})$
- Many Sy 1s and 2s have very weak Si strength (e.g., Roche et al. 1991, Shi et al. 2006, Hao et al. 2007).
- Si strength is a constraint on torus models (e.g., Pier & Krolik 1992; Laor & Draine 1993).

(Left). Average spectra of QSOs (red), Seyfert 1s (green), Seyfert 2s (blue), and ULIRGs (black).. The 10 µm silicate strengths measured from the average spectra are: 0.20, -0.21, -0.54, and -1.44 for quasars, Seyfert 1s, Seyfert 2s, and ULIRGs, respectively.

(Right) Distribution of the 10 µm silicate strength, S10, for QSOs, Seyfert 1s, Seyfert 2s, and ULIRGs. Silicate absorption increases to the right. In QSOs, Seyfert 1s, and Seyfert 2s, the distributions of sources that are also in the ULIRG sample are shaded. The averages of the 10 µm silicate strengths are 0.20 for quasars, -0.18 for Seyfert 1s, -0.61 for Seyfert 2s, and -1.56 for ULIRGs. (Hao et al. (2007).

The Clumpy Torus

In the clumpy torus, dust at a range of temperatures is seen, so there is less change with orientation than in uniform models.

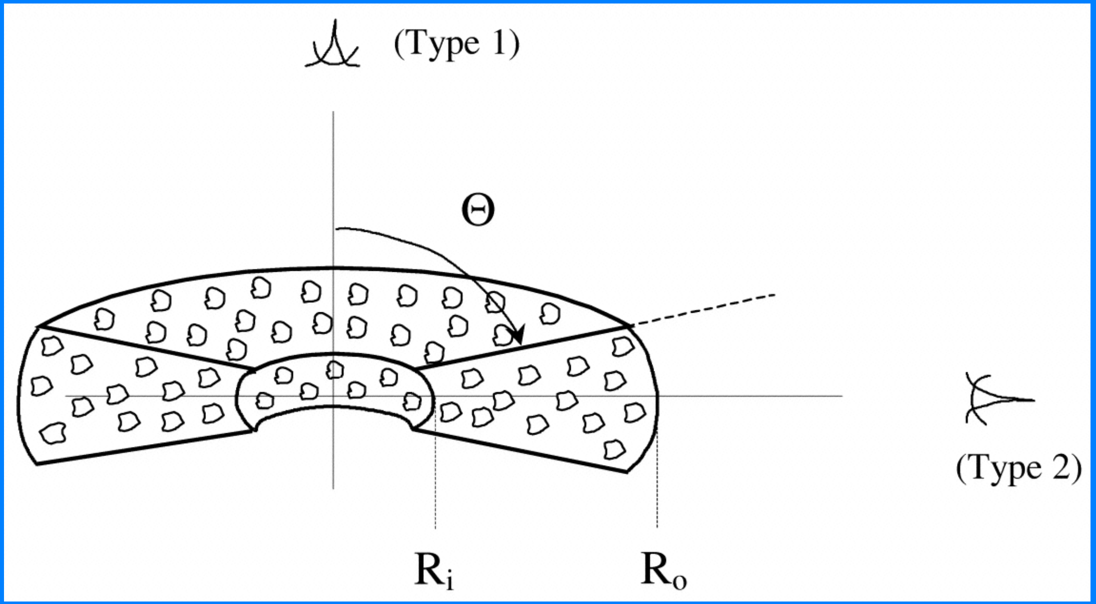

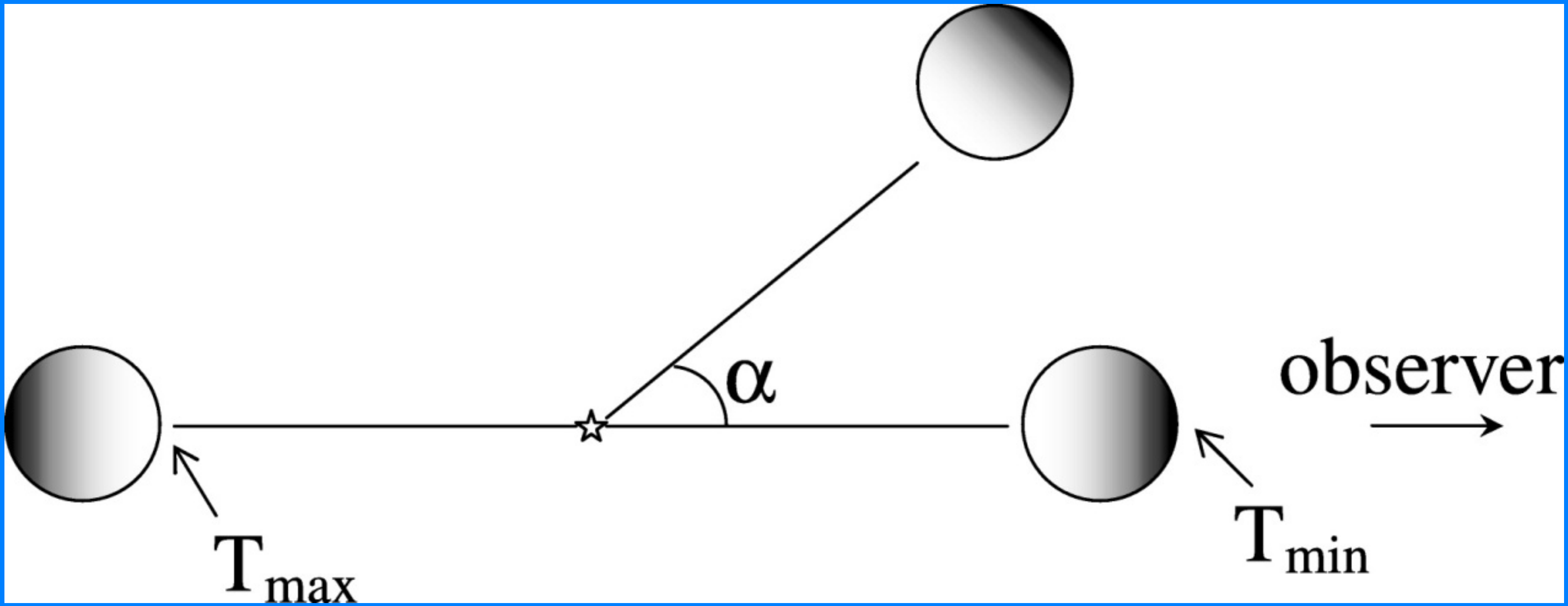

Nenkova et al. 2008

Near-IR Cont and Sil Strength are Torus Orientation Indicators

- Smooth density torus models predict large changes in relative brightness of near IR emission and 9.7 µm Sil as a function of inclination to e torus axis (e.g., Rowan-Robinson & Crawford 1989; Pier & Krolik 1993; Siebenmorgan et al. 2004).
- Clumpy torus models predict much smaller changes in relative brightness of near IR emission as a function of inclination (Nenkova et al. 2002).

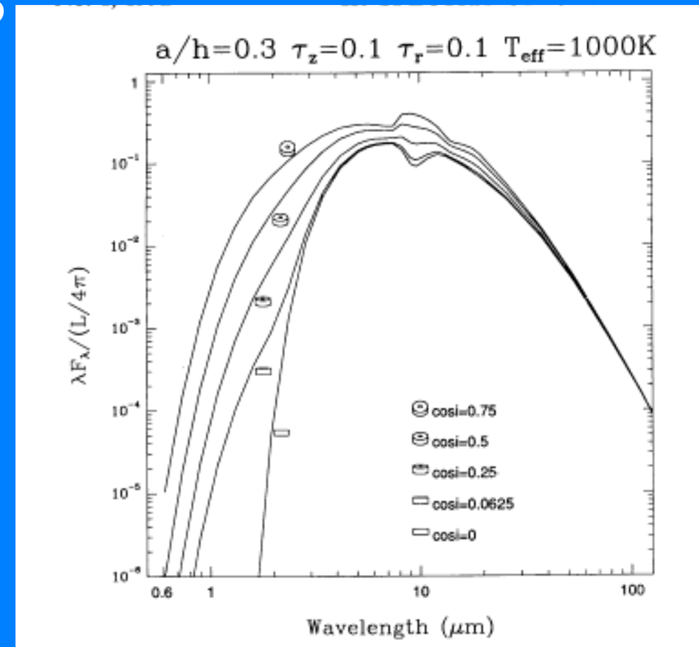

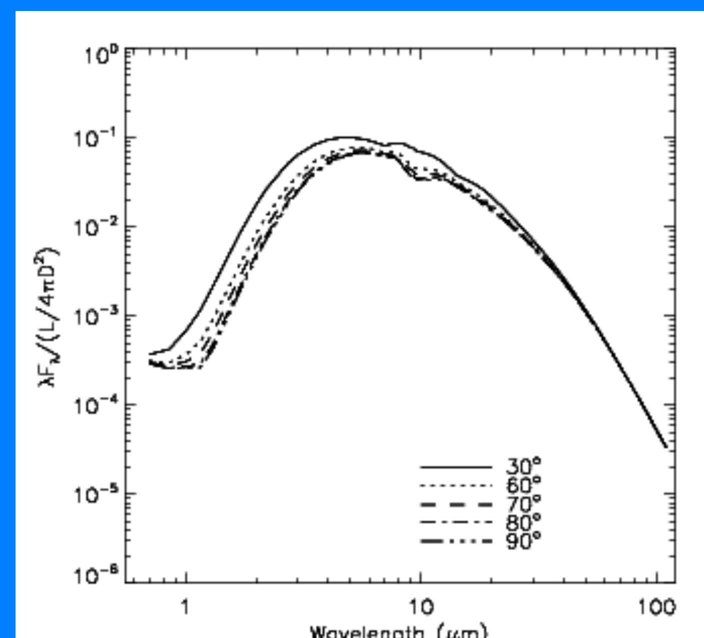

(Top). Pier & Krolik 1992 ApJ 401, 99, constant-density modle. The parameters used are: a/h=0.3, where a = inner radius of torus, h = height of torus, vertical optical depth of 0.1, radial optical depth of 0.1, and T$_{ef}$f (inner torus temperature) of 1000K. (Bottom). Clumpy torus model from Nenkova et al. 2002 ApJ 570 L9. The particular model used is TAB-N10q2-sig45p2-D.tv10, i.e.: no direct AGN emission, 10 clumps along the line of side, radial density distribution of clumps going as r^{-2}, 45° opening angle of the torus, Gaussian vertical distribution of clumps, and optical depth (V) of 10 for individual clumps.

Fine-Structure (Forbidden) Lines

- We will use high ionization lines as AGN tracers
- [OIV] 26 µm (54.9 eV)
- [NeV] 14, 24 µm (97.1 eV)

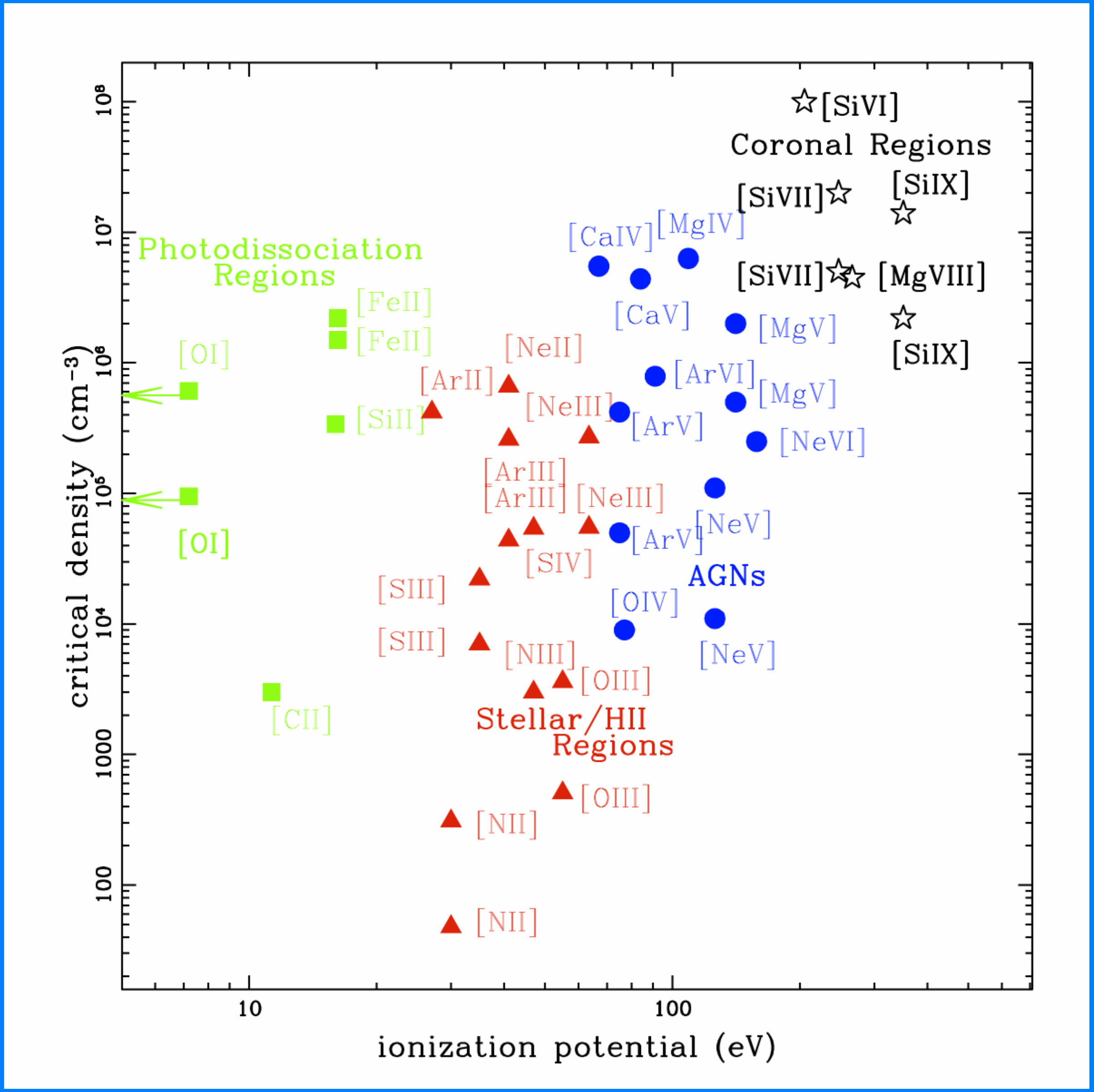

IR diagnostic fine-structure lines in the range 3 – 200 µm (Spinoglio 2009).

Polycyclic Aromatic Hydrocarbons (PAH)

- Made of Benzene Rings
- Formed in dusty ISM regions
- Absorb UV photons and then radiate in the near-mid IR via stretching and bending modes
- PAH is a tracer of Star formation (e.g., Tielens et al 1999; Laurent et al 2000; Peeters et al 2004)
- PAHs may be destroyed by AGN (Voit 1992)

Benzene

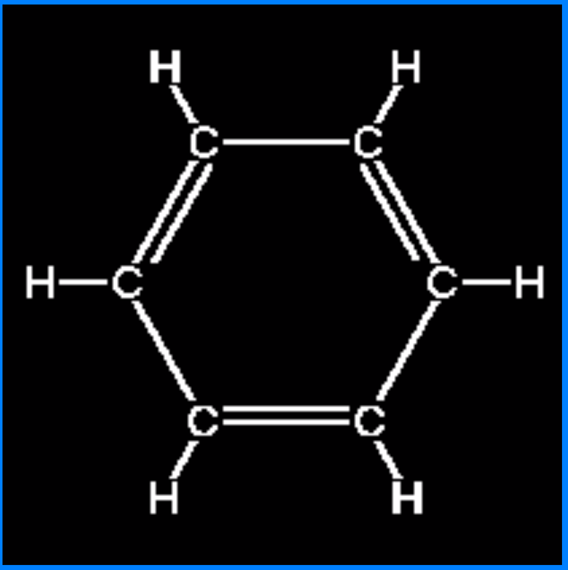

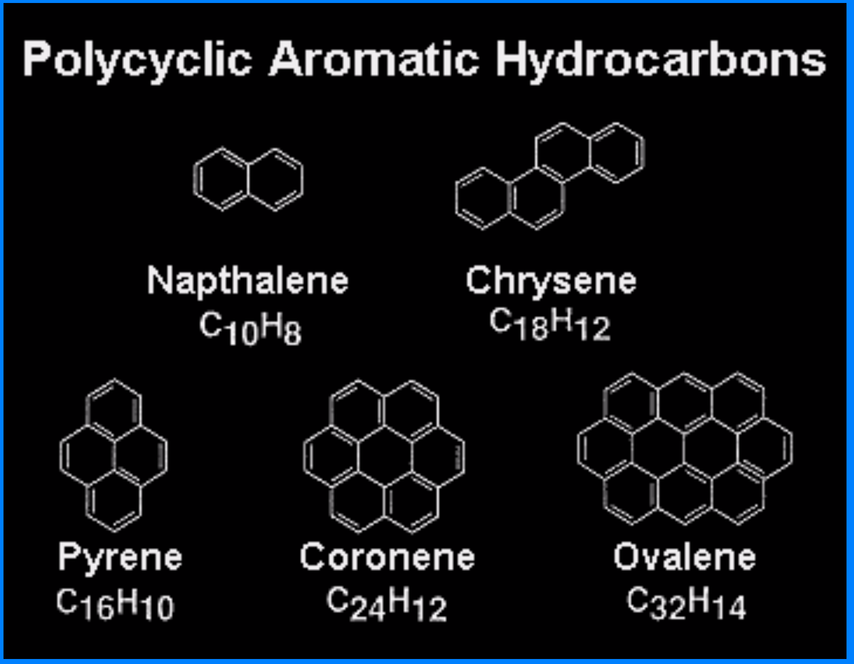

Figures from Sloan (2007)

Mid-IR Diagnostics using PAHFIT

- Smith & Draine's PAHFIT (slightly modified) used to fit the IRS Spectra
  - Continuum approximated by a series of grey bodies at a range of Temp.
  - Comprehensive set of PAH, Si, forbidden lines

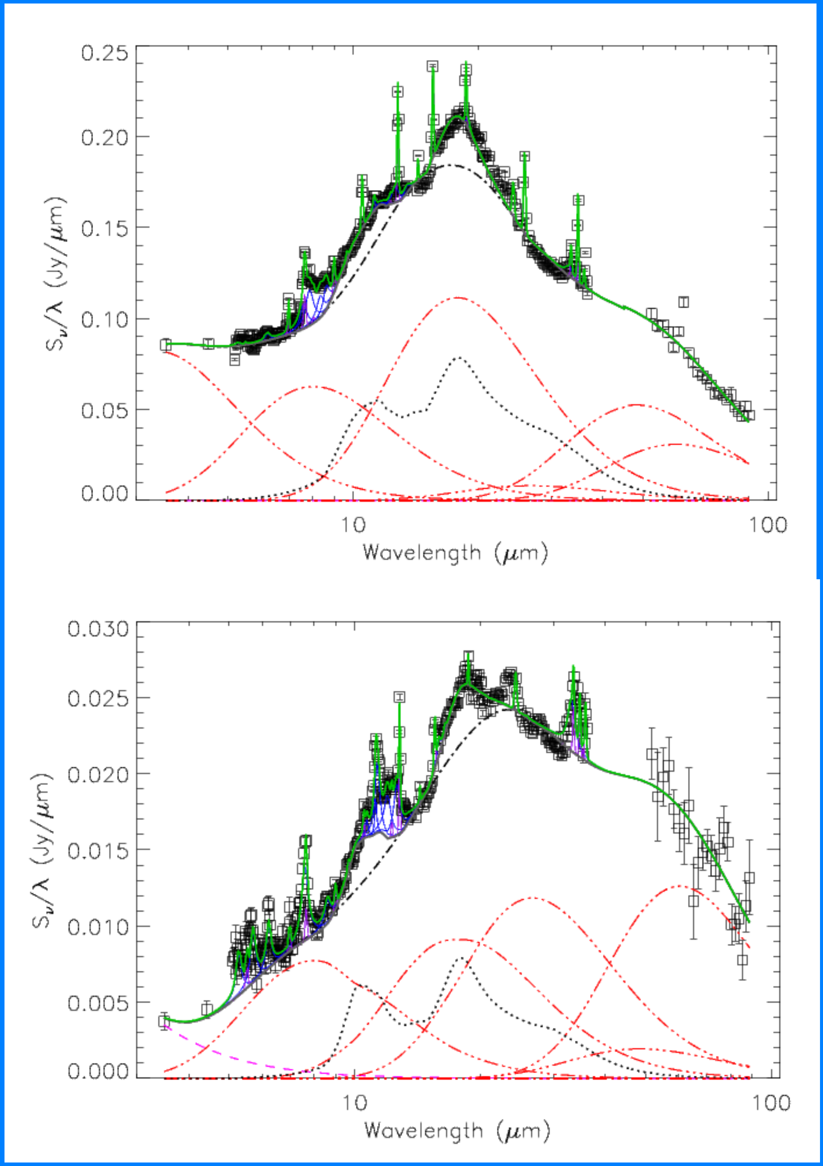

PAHFIT spectrum decomposition. (Left) NGC 4151. (Right) (NGC7213). Data are squares. Continuous lines: Green - best fit model, dust - grey, PAH - blue, emission lines - purple; broken lines: stars – pink dashed, dust continuum – red dash-dot-dot-dot, optically thin warm dust emission – black dots. The baseline used for the Sil index measurements (stars + dust continuum + warm, thin dust) – black dash-dot-line. (Gallimore et al. 2010).

Wide Variety of SEDs Seen in AGN

Large differences in relative amounts of cold and hot dust in the SED.

"Torus" must be optically thick out to at least 10 μm.

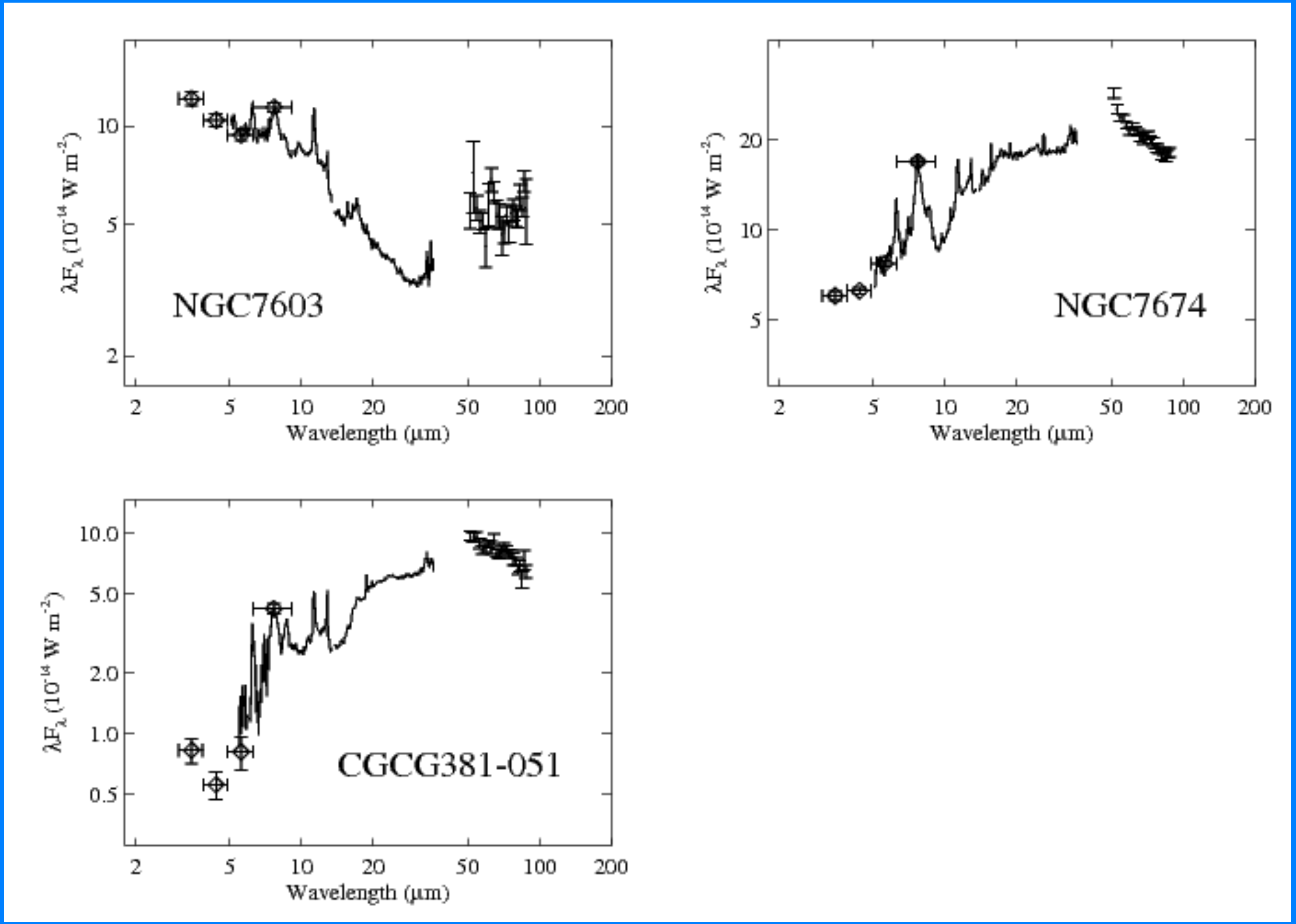

Seyferts from the Extended 12 μm sample (Rush + 1993). SEDs are plotted as λF_λ vs. rest λ, in RA order. IRAC and IRS extracted from 20" diameter synthetic aperture, MIPS SED from 30" aperture along 20" wide slit. (Gallimore+2010).

Large Radio Galaxies

Quasars and (Some) Radio Galaxies Have Comparable Central Engines

Mid-IR luminosities "comparable" in powerful RG and quasars (Haas+2005, Ogle+2006).

Ratio of high and low ionization lines comparable in powerful RG and quasars (Haas+2005).

Some radio galaxies have much lower mid-IR luminosities (the LEGs) (Ogle+2006).

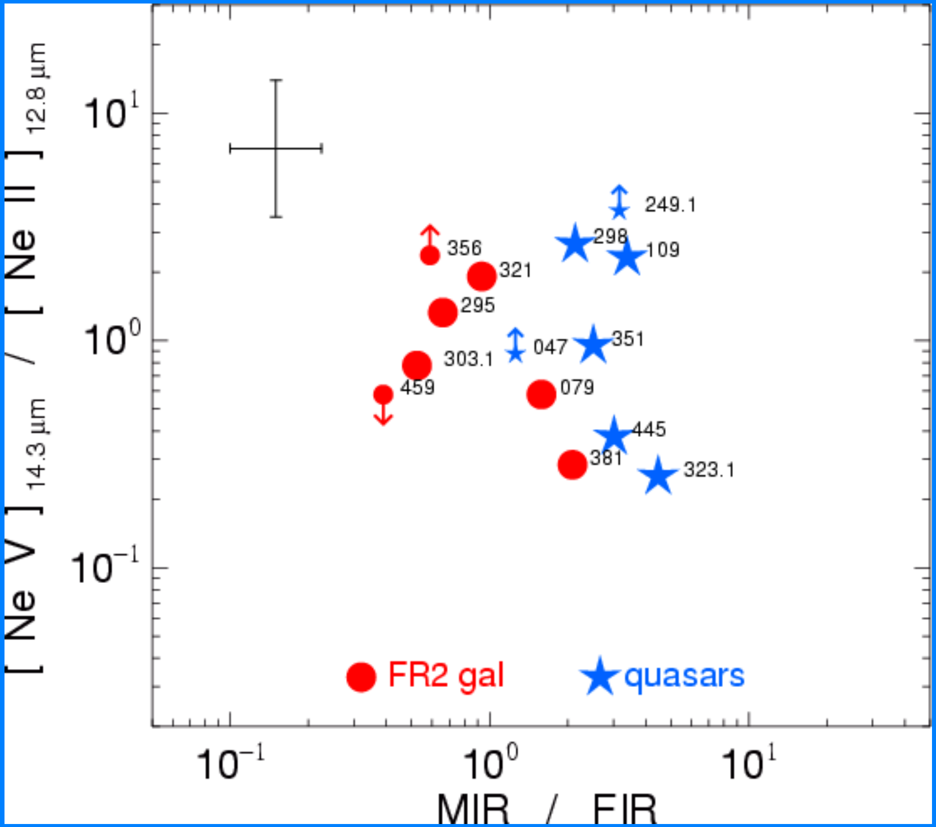

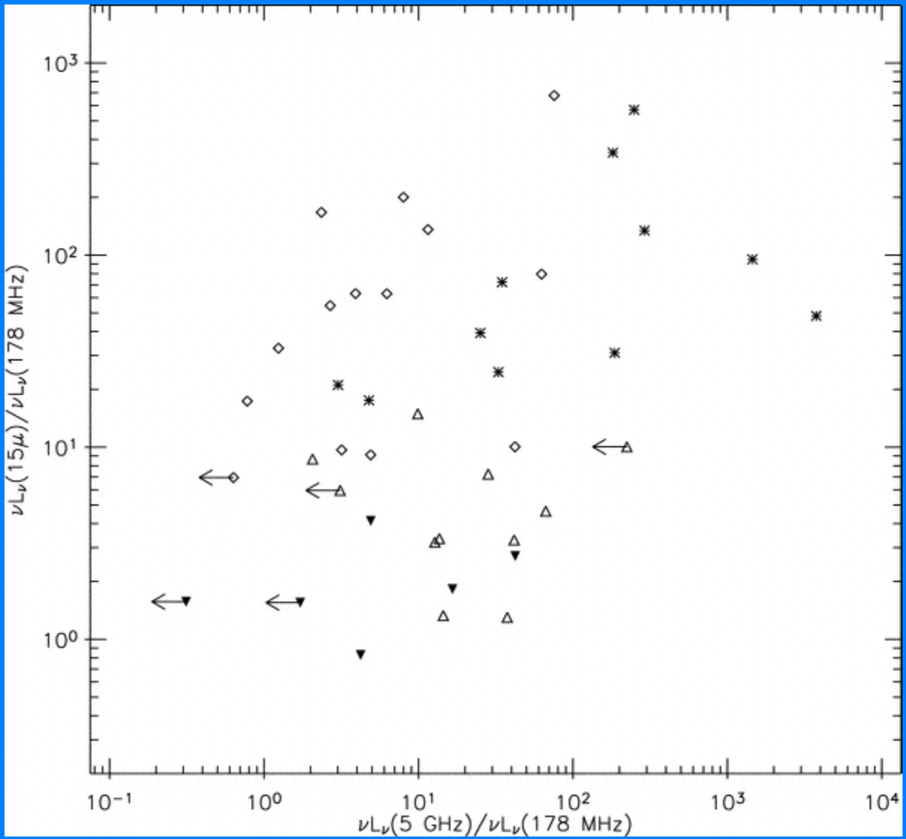

(Top) Luminosity ratios of high over low excitation lines versus mid-to far-infrared luminosity for powerful 3CR sources (Haas+ 2005). (Bottom) Mid-IR (15 µm, rest) luminosity vs. 5 GHz (observed) radio core luminosity, both normalized by 178 MHz (rest) radio lobe luminosity. The various symbols represent mid-IR weak NLRGs (open triangles), upper limits (filled triangles), mid-IR luminous NLRGs (diamonds), and quasars (asterisks). Upper limits at 5 GHz are indicated by arrows. The most core-dominant sources, with νL_ν(5 GHz)/νL_ν(178 MHz)> 10^2 are all quasars or BLRGs. (Ogle+ 2006).

Torus Extinction
$A_v \sim 20$

Difference between Quasar and Radio Galaxy mid-IR spectra consistent with $A_v \sim 20$ for $1 < z < 1.4$ 3CRR sources (Leipski+2010) .

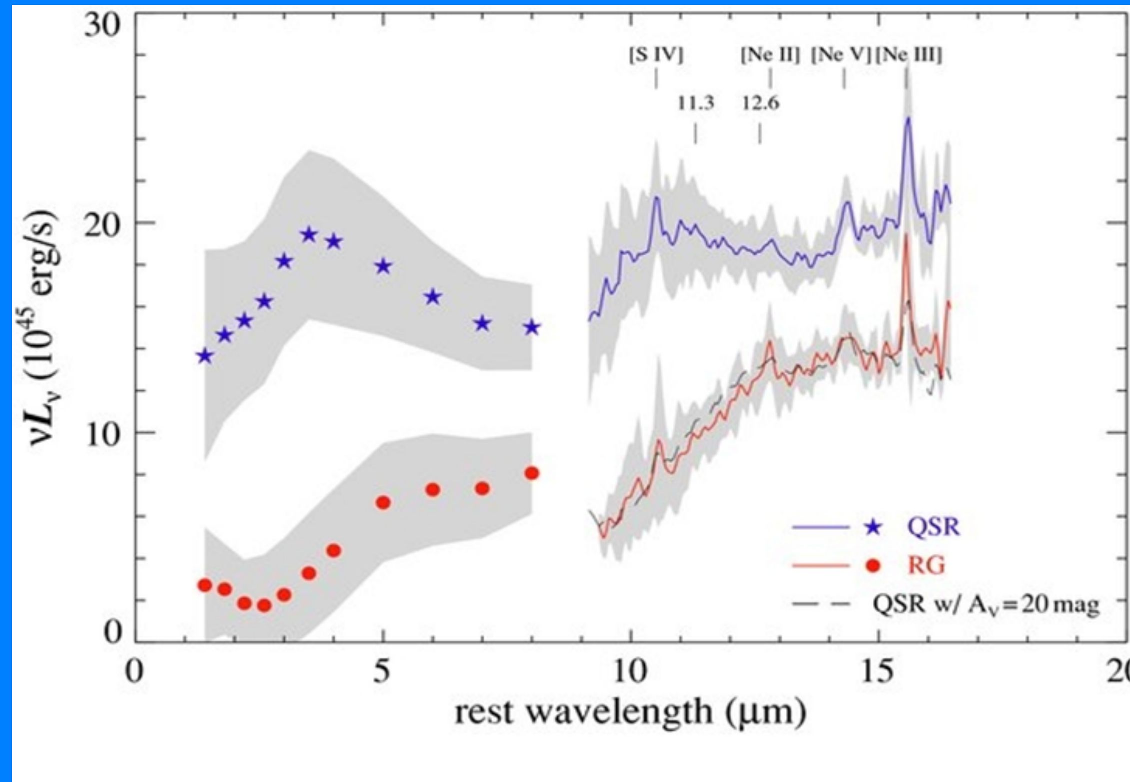

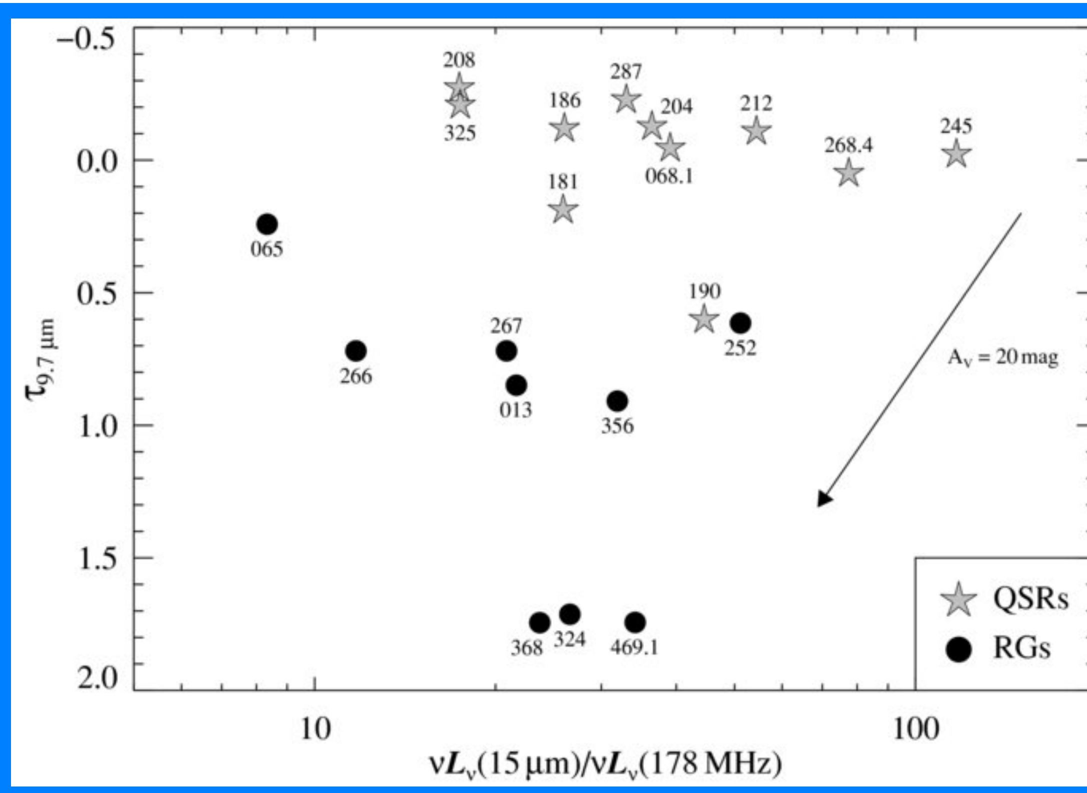

(Top) (Average 9–16 μm spectra of the high-z 3CRR sources supplemented by 1–8 μm photometry. The solid lines represent the average spectra while the symbols indicate the average photometry. The SEDs are normalized to the isotropic low-frequency radio luminosity. The black dashed line represents the average quasar spectrum reddened by a dust screen of $A_V = 20$ mag without any additional scaling. The shaded areas indicate the 1σ dispersion.Bottom) Low-frequency normalized luminosity at 15 μm plotted vs. the depth of the silicate feature. The arrow shows the effect of a dust screen with $A_V = 20$ mag, assuming the Chiar & Tielens (2006) extinction curve. Dereddening the radio galaxies along the direction of the AV arrow shifts them to the same normalized L15μm range as populated by the quasars. (Leipski+2010).

[OIII]λ5007Ả is not Completely Isotropic. I

[OIII]λ5000Ả/[OIV]λ 25.9 μm higher in quasars than in Radio Galaxies (Haas+2005)

Mid IR/[OIII]λ5007 lower in quasars than RGs (Dicken+2009)

Suggest that some of the [OIII] is emitted in regions obscured by the "torus".

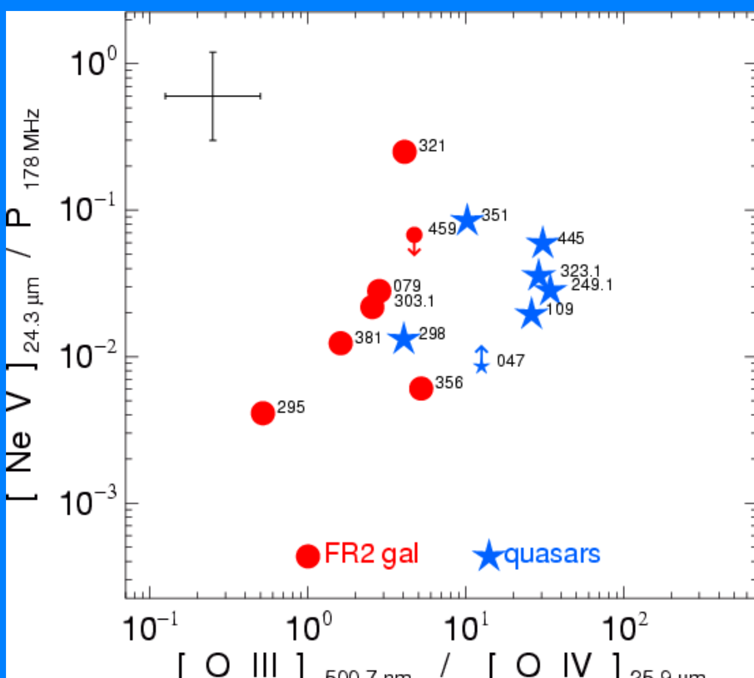

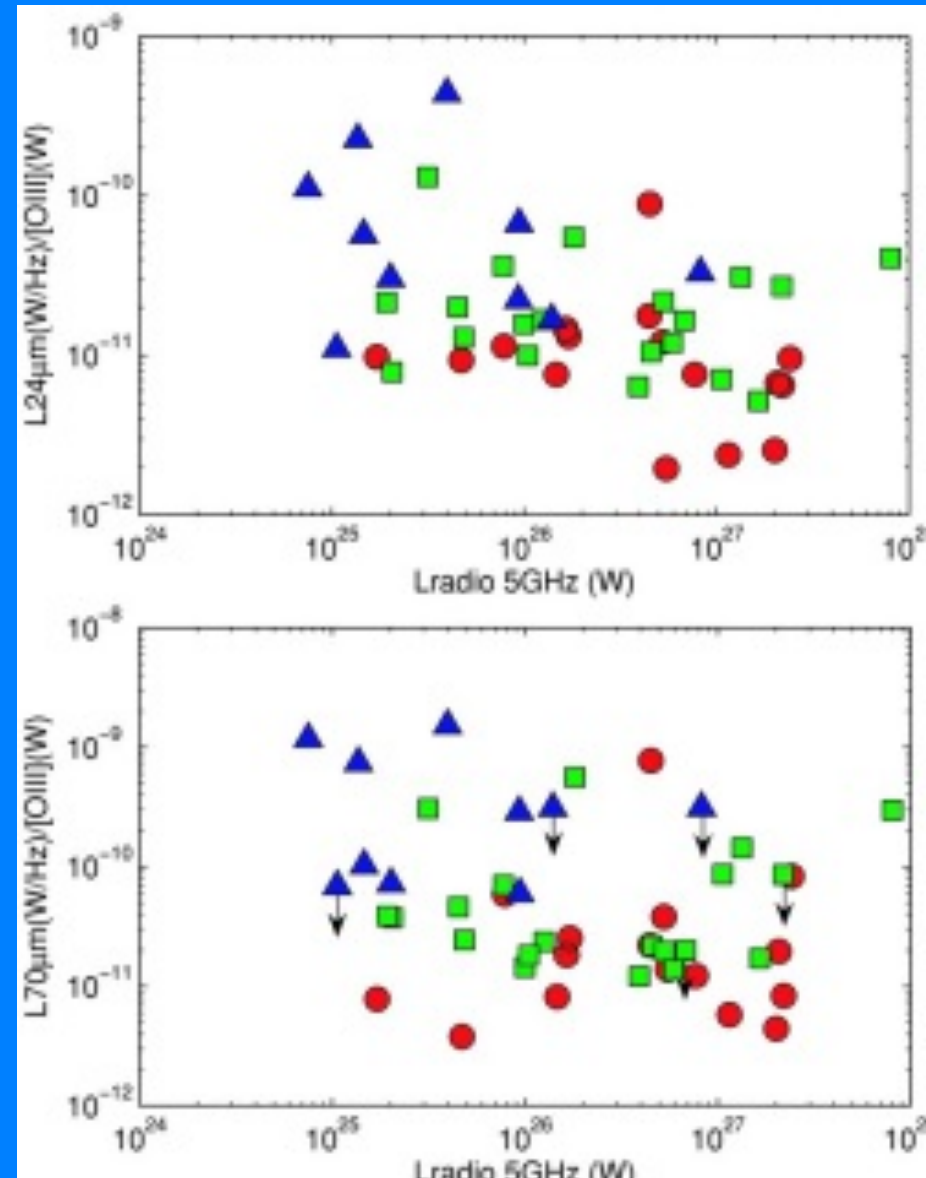

(Top) High-excitation line to radio luminosities versus [OIII] λ5007Ả / [OIV]λ25.9μm luminosities (Haas+2005). (Bottom) Plots of 24 μm (top) and 70 μm (bottom) luminosities normalized by [O iii]λ5007 luminosity vs. 5 GHz radio total radio luminosity. Red circles indicate BLRG/Q objects, green squares NLRG, and blue triangles WLRG. (Dicken+2009)

[OIII]λ5007Å is not Completely Isotropic. II

[OIII]λ5000Å/[OIV]λ 25.9 μm is a function of Si (9.7 μm) and is higher in Seyfert 1s than Seyfert 2s (Baum+2010) and is higher in BLRGs and Quasars than in NLRGs (Dicken+2014).

This suggests that some of the [OIII] is emitted in regions obscured by the "torus".

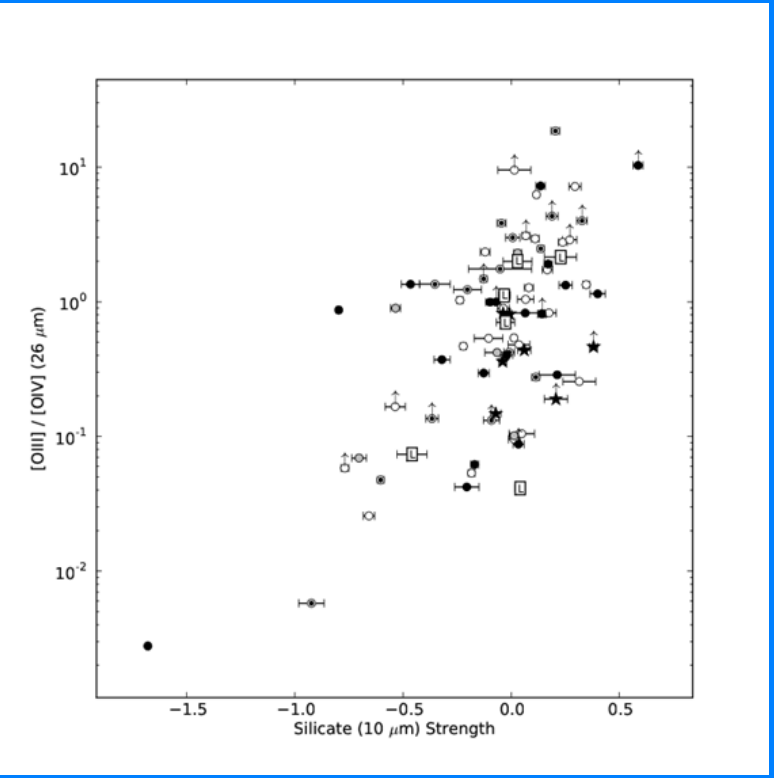

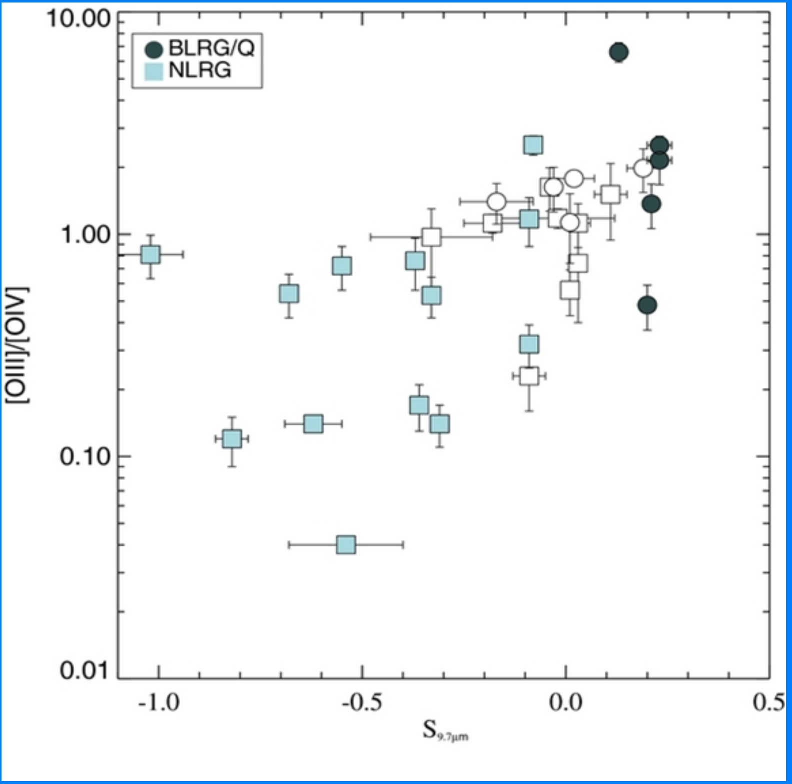

(Top) [OIII] λ5007Å / [OIV]λ25.9μm vs Si (9.7μm) strength – here used as an orientation indicator. Sy 1-1.5: open circles, Sy 1.8,1.9 : gray-filled circles, Sy 2: filled circles, HBLR Sys (Sy 1h, and S1i): partially filled circles, LINERS: squares labled "L", Starburst/HII: stars. Limits are indicated by appropriately directed arrows. (Baum+ 2010). (Bottom) Plot of S9.7 vs. [O III]/[O IV]. Filled squares are narrow-line radio galaxies; filled circles are broad-line radio galaxies. Unfilled objects are undetected in S9.7, i.e., below 3σ. The sample is 46 2Jy radio galaxies (0.05 < z < 0.7) and 17 3CRR FRII radio galaxies (z < 0.1) (Dicken+2014).

The AGN Heats the Dust in Radio Galaxies

In the 2Jy and 3CRR Sample, the dust emission at 24 and 70μm is correlated with the [OIII] λ5007 luminosity (which is an AGN tracer) suggesting that the dust emission is also an AGN tracer (Tadhunter+2007, Dicken+ 2009, 2010).

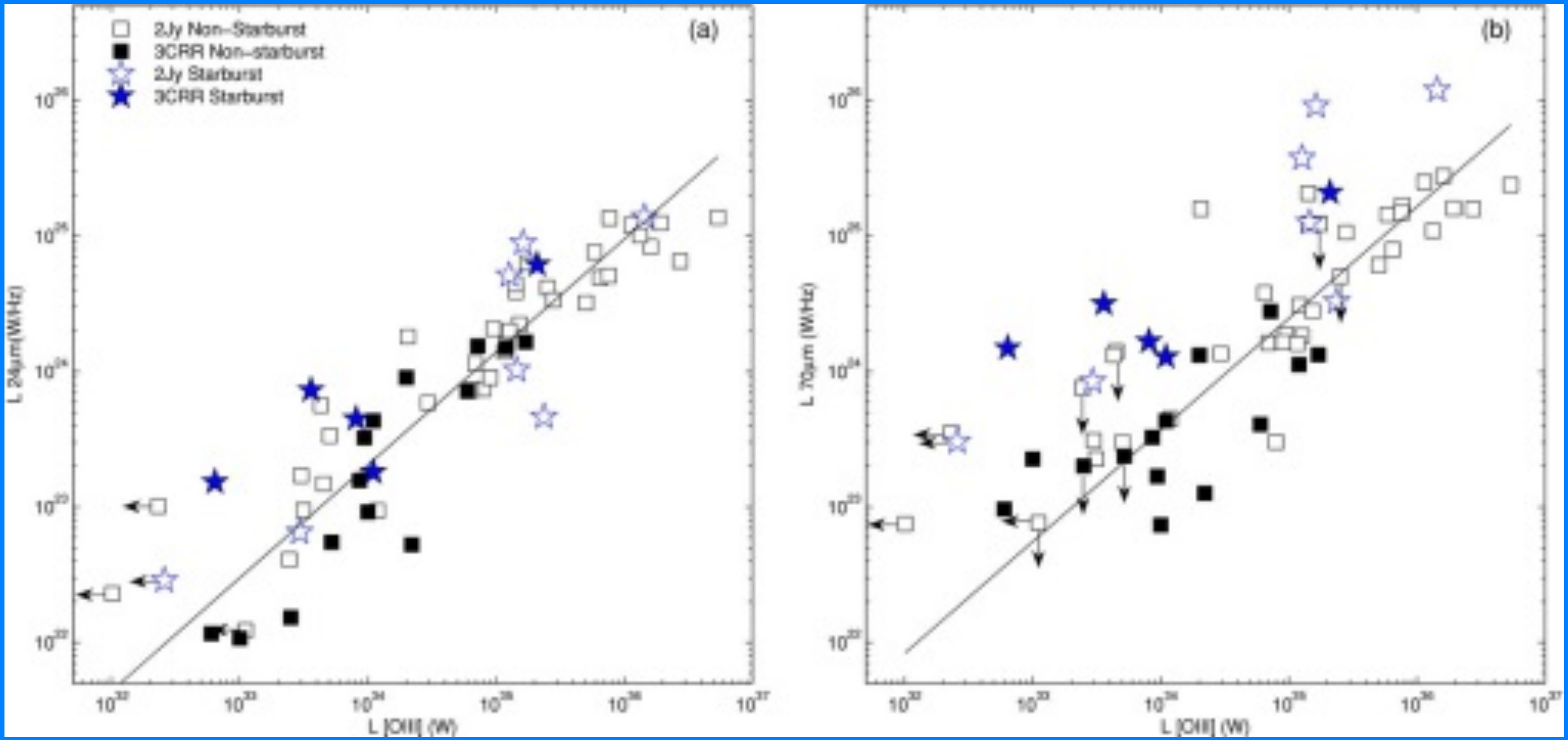

Plots showing the correlations between MFIR and [O III] luminosity for the combined 3CRR and 2 Jy sample at (a) 24 μm and (b) 70 μm, with optical starbursts marked with separate symbols (blue stars). The regression line is fitted to the entire 3CRR sample as well as the 2 Jy sample objects with z > 0.06 in order to avoid most of the objects with upper limits in [O III]. (Dicken+2010).

Most FRIs Lack the AGN-Heated Dust

Spitzer IRS study of sample of 25 FRIs (Leipski+2009). I removed the two Type-1 objects and BL Lac.

AGN heated dust found in 4/22 (18%)

Significant star formation found in 8/22 (36%)

Non-thermal component found in 9/22 (41%) and in 8/11 (73%) of FRIs with optical compact core.

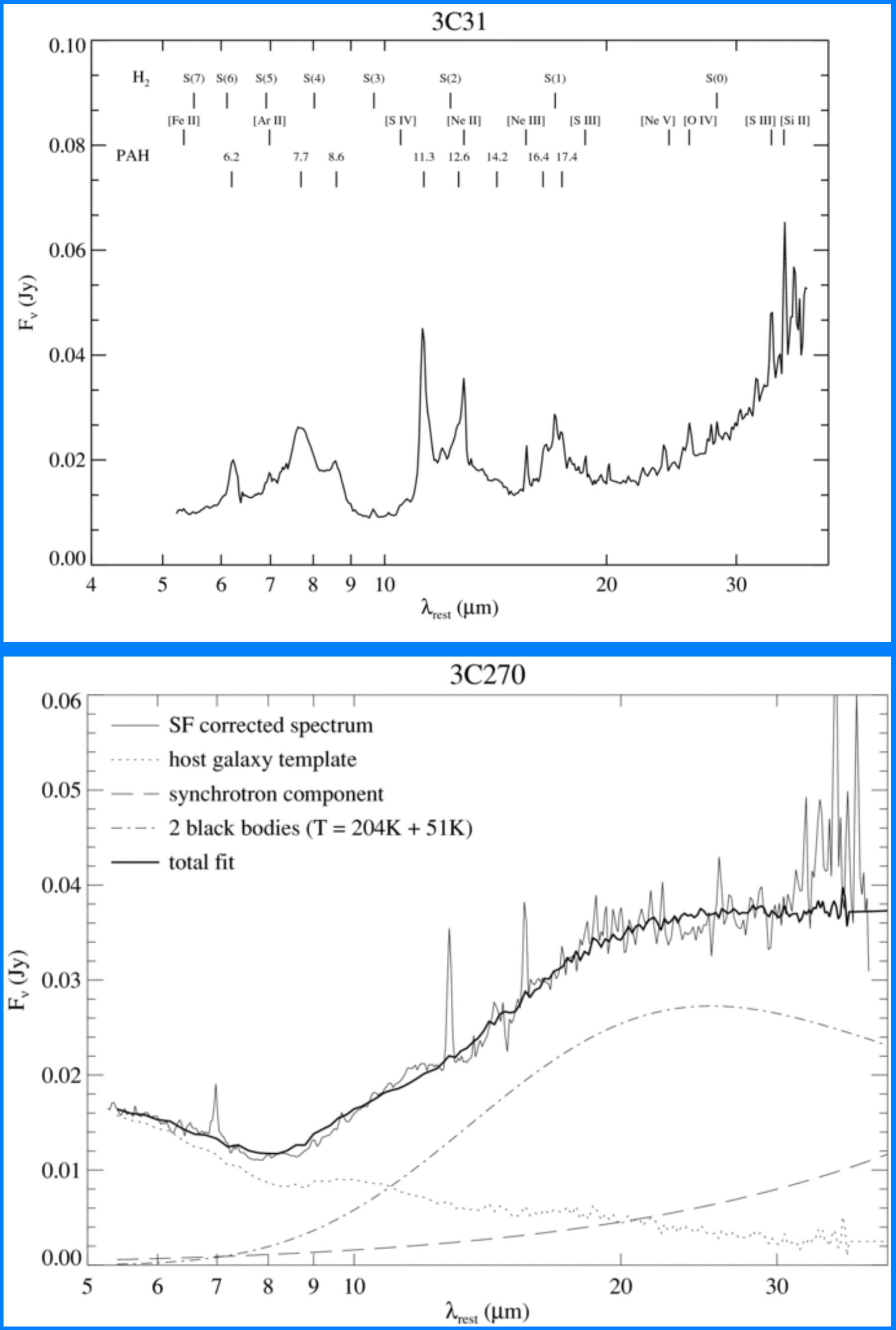

(Top) 3C31. Spitzer IRS spectrum showing only the host galaxy + star formation. (Bottom) 3C270. Model fitting to Spitzer IRS spectrum showing warm dust and non-thermal component (Leipski +2009). Significant contribution to the SED is defined to be > 30% at 30μm (O'Dea 2015)

Weak Line Radio Galaxies are Intrinsically Weak

In the 2Jy + 3CRR FRII sample, the other AGN tracers correlate with L[OIV] and WLRGs have the lowest values of the AGN tracers.

Since the optical depth of the torus at [OIV] 25.9 µm should be low, this indicates that the WLRGs are intrinsically weak (Dicken+2014).

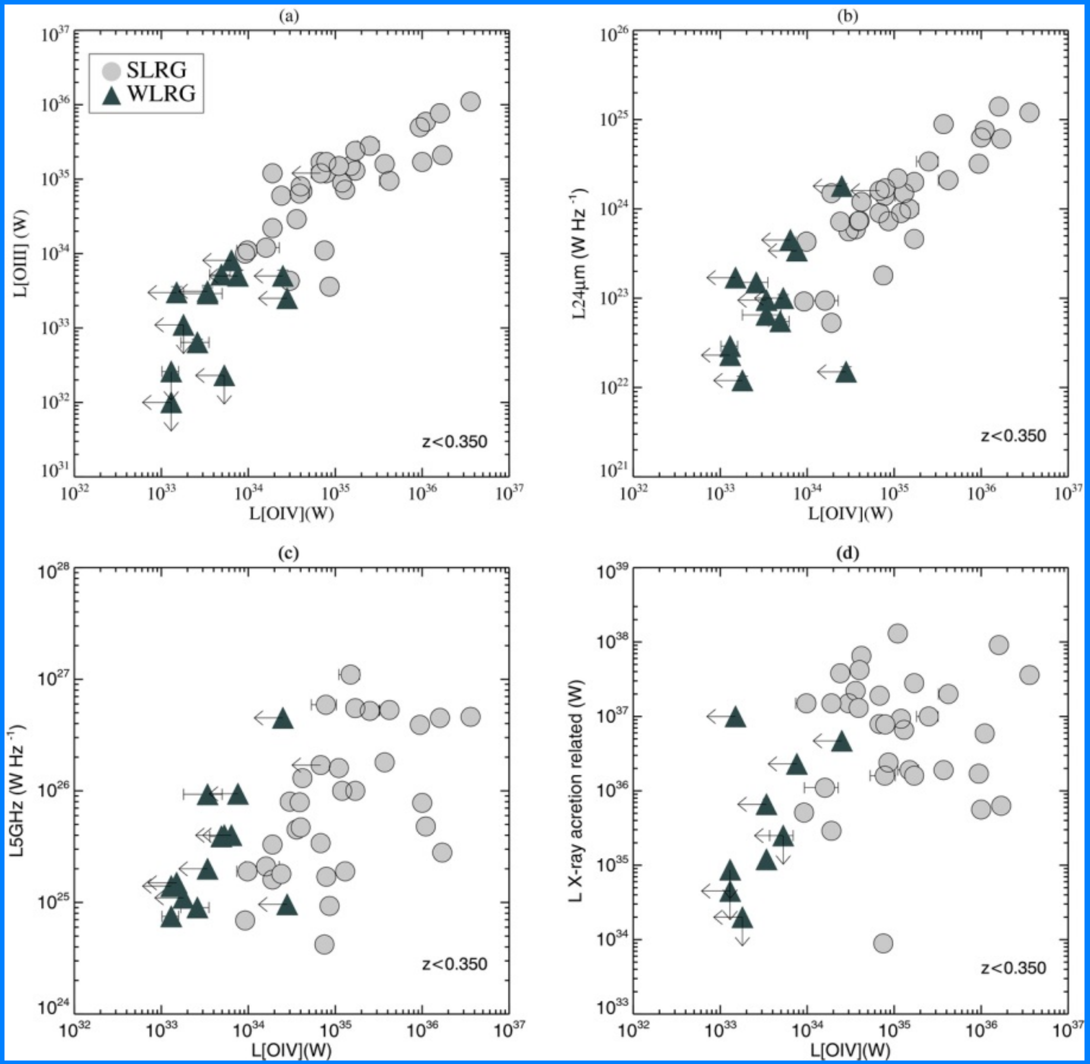

Plot showing L[O IV] λ25.89 µm vs. L[O III] λ5007, L24 µm, L5 GHz, and L[Ne III] λ15.56 µm with objects identified as strong-line radio galaxies (SLRG) or weak-line radio galaxies (WLRG). The objects plotted are limited to objects with z < 0.350 because of the [O IV] line redshifted out of the redshift range of Spitzer/IRS. SLRG: strong-line radio galaxies/quasars. (Dicken+2014)

3C Star Formation Rate is Moderate

Star formation rate decreases from 2MASS to PG to 3C (Shi+2007).

Contribution of star formation to the SED increases with increasing wavelength. The average star formation fractions for the whole sample at MIPS 24, 70, and 160 µm are 4%, 26%, and 28% (Shi+2007)

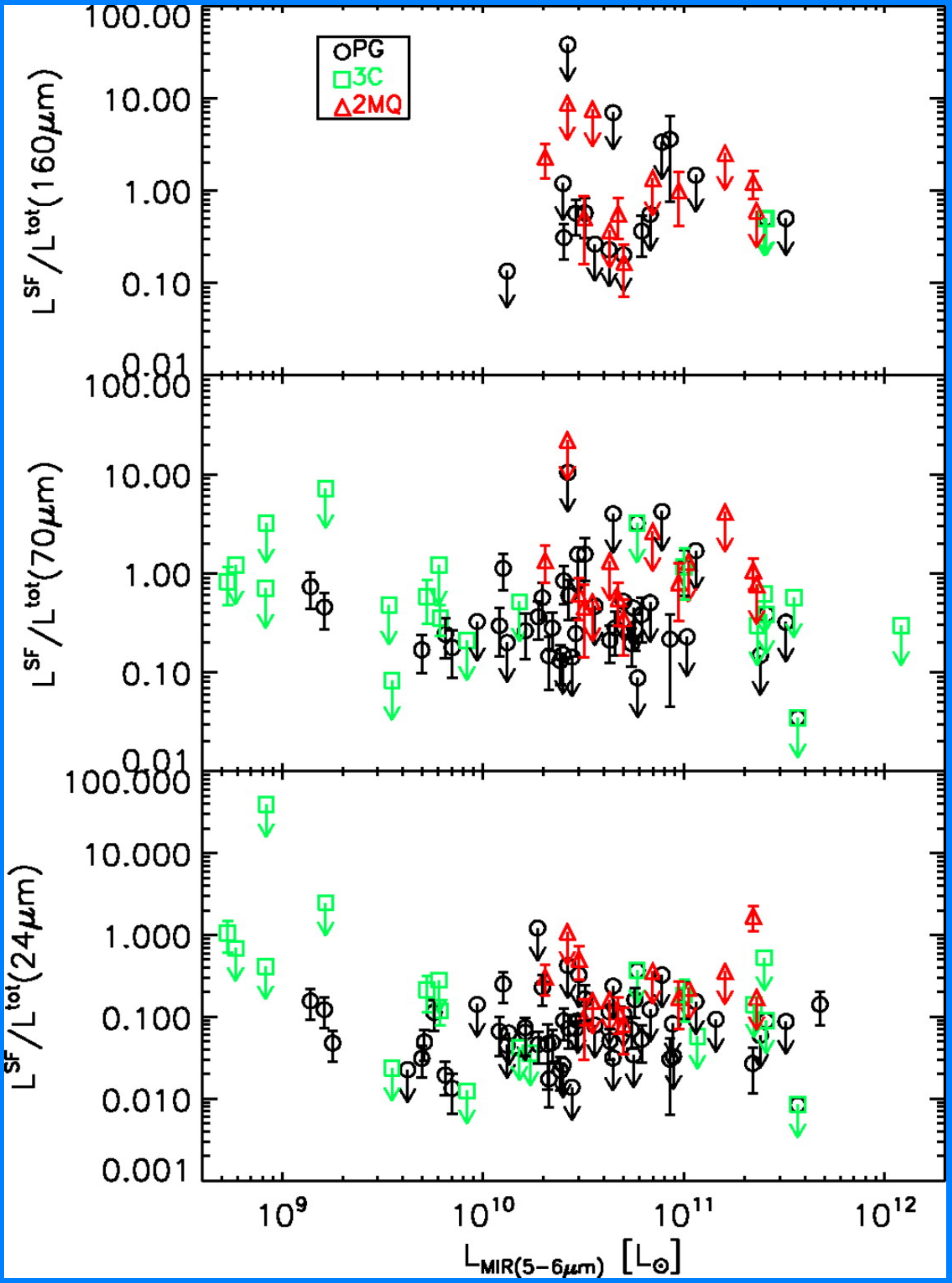

Star formation fraction at 24, 70, and 160 µm vs. the mid-IR (5–6 µm) luminosity for the PG quasars, 2MASS quasars and 3C radio galaxies + quasars (Shi+2007).

RGs Have Moderate to Low Star Formation

~30% of (z<0.22) radio galaxies show high H_2 luminosities. The H_2 may be heated by radio jet feedback (Ogle+2010).

Ratio of PAH 11.3/L(24μm) indicates low to moderate star formation rates (Ogle+2010)

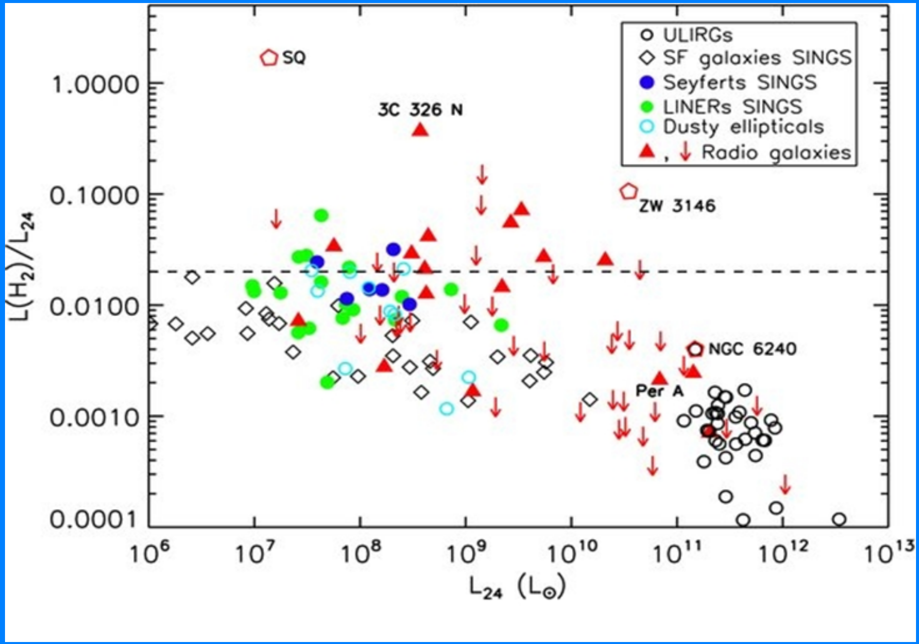

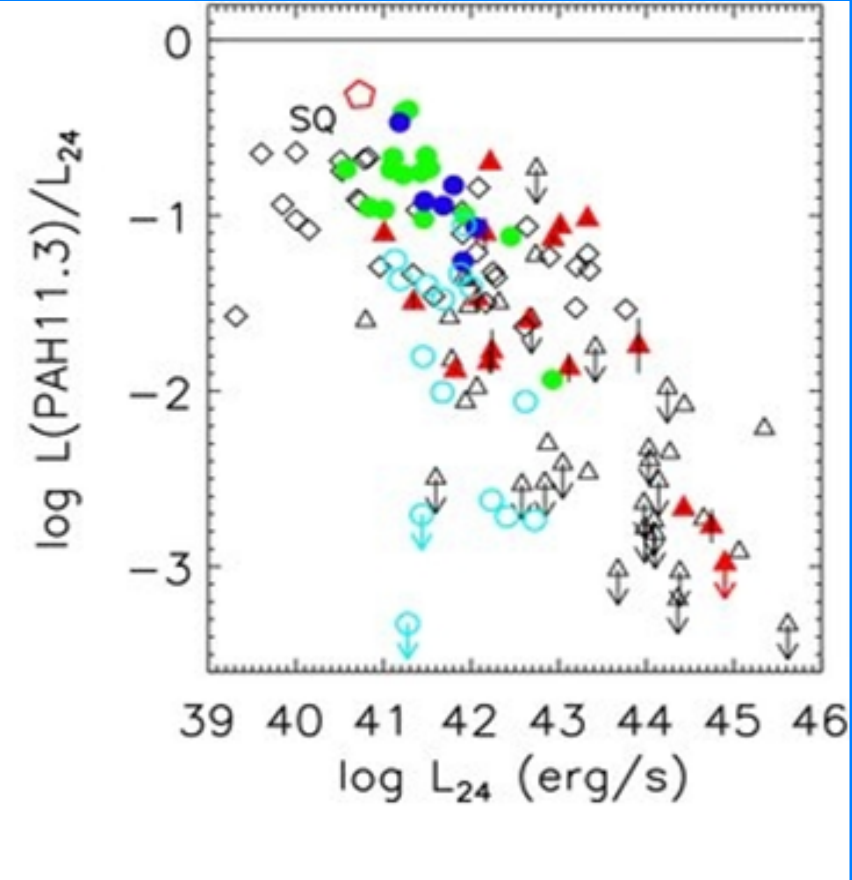

(Top) Ratio of H2 luminosity summed over the 0–0 S(0)–S(3) pure-rotational lines to L24 = νLν(24 μm, rest) luminosity. Radio galaxies (this work) are compared to SINGS star-forming galaxies, Seyferts, and LINERs (Roussel et al. 2007), ULIRGs (Higdon et al. 2006), and the subset of Kaneda et al. (2008) dusty ellipticals that have 24 μm Spitzer MIPS fluxes (Temi et al. 2007). (Bottom) PAH to νLν(24 μm, rest) luminosity ratio, for the 11.3 μm PAH feature. H_2 nondetected radio galaxies are plotted as open triangles. Solid line corresponds to 1:1 ratio. (Ogle+2010)

Summary of Large Sources

The IR data are consistent with the basic unification picture for radio galaxies and quasars (e.g., Antonucci 1993, Barthel 1989)

However, there is a population of Weak Line radio galaxies (some FRIIs, most FRIs) which do not have a hidden quasar nucleus. This is consistent with work in the optical and X-ray which suggests two different accretion modes (e.g., Baum+1995, Hardcastle+2009, Buttiglione+2010)

[OIII] emission is partially obscured by the "torus".

Star formation rates in powerful radio sources tend to be less than in other types of AGN (PG and 2MASS quasars). This result, combined with the evidence for shock heated H_2 is consistent with some radio source feedback.

GPS/CSS Sources

Nearby CSO Sample (Willett +2010)

PAH detected in all 7 CSO

[NeV] not detected, but [OVI] detected in 6/7

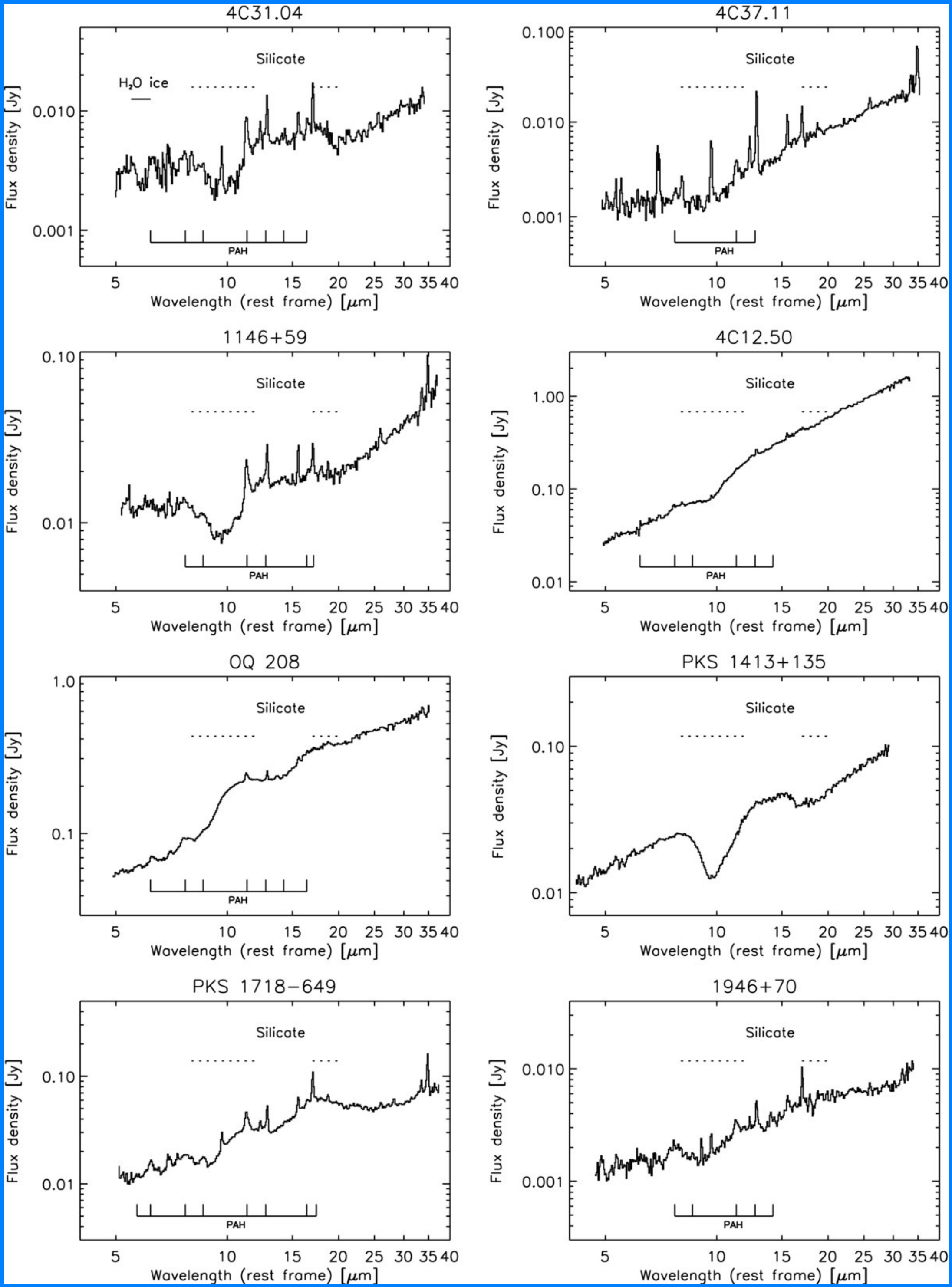

7 CSOs z < 0.1. The photometrically scaled LR spectra with individual modules stitched together. (Willett+2010). I will ignore the BL Lac object 1413+135.

The CSO Sample

Table 1
Properties of CSOs Observed with *Spitzer* IRS

Object	R.A. (J2000.0)	Decl. (J2000.0)	$z_\odot$	D_L (Mpc)	H I Column (cm^{-2})	H I Ref.	Optical Spec.	Optical Ref.	log P_{radio} (W Hz^{-1})	log L_{IR} ($L_\odot$)	log L_X ($L_\odot$)
4C +31.04	01 19 35.0	+32 10 50	0.0602	264	1.08×10^{21}	1	WLRG	8	25.34	10.60	...
4C +37.11	04 05 49.2	+38 03 32	0.055	242	1.8×10^{20}	2	NLRG	9	25.05	...	...
1146+59	11 48 50.3	+59 24 56	0.0108	48.2	1.82×10^{21}	1	LINER	10	23.10	9.09	...
1245+676[a]	12 47 33.3	+67 23 16	0.1073	495	6.73×10^{20}	3	WLRG	8	25.02	...	...
4C +12.50	13 47 33.3	+12 17 24	0.1217	571	$T_s 6.2 \times 10^{18}$	4	NLRG	11	26.30	12.15	43.3
OQ 208	14 07 00.4	+28 27 15	0.0766	349	1.83×10^{20}	5	BLRG	12	25.08	11.33	42.7
PKS 1413+135	14 15 58.8	+13 20 24	0.2467	1244	4.6×10^{22}	6	BL Lac	13	26.31	11.97	44.4
PKS 1718−649	17 23 41.0	−65 00 37	0.0142	62.6	...	...	LINER	14	24.25	...	...
1946+70	19 45 53.5	+70 55 49	0.1008	460	2.2×10^{23}	7	...	15	25.39	...	...

Note.
[a] Undetected with the spectral modules on the IRS; see Section 3.1.

References. (1) van Gorkom et al. 1989; (2) Maness et al. 2004; (3) Saikia et al. 2007; (4) Mirabel 1989; (5) Vermeulen et al. 2003; (6) Perlman et al. 2002; (7) Peck et al. 1999; (8) Marchã et al. 1996; (9) Rodriguez et al. 2006; (10) Kim 1989; (11) Baan et al. 1998; (12) Petrosian et al. 2007; (13) Stocke et al. 1992; (14) Filippenko 1985; (15) Snellen et al. 1999.

Diverse mid-IR Spectra

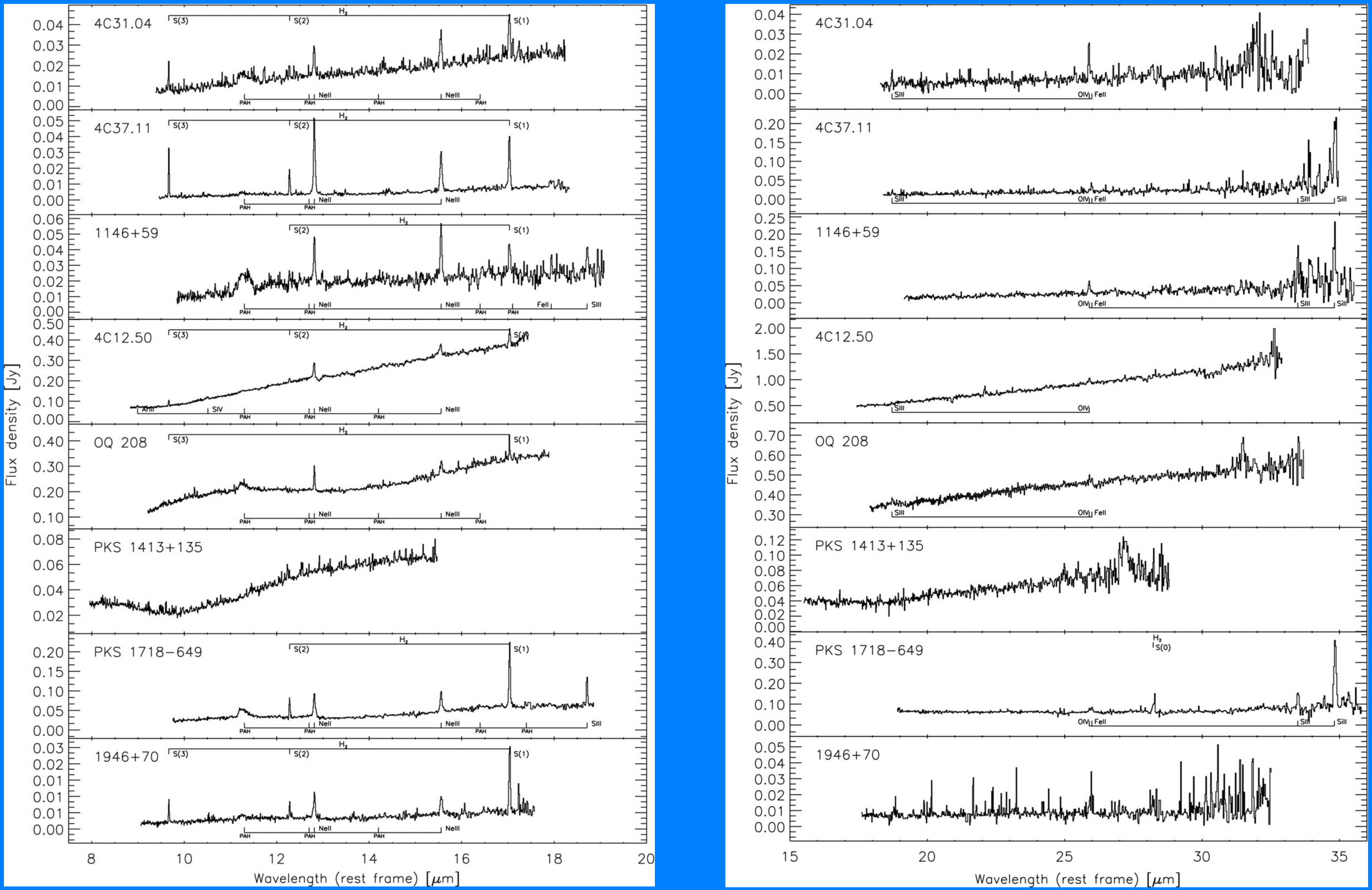

High resolution IRS spectra (Willett+2010).

CSOs Have Enhanced Star Formation

Ratio of high to low excitation lines, and Ratio of 15/5.5 μm flux vs. PAH 6.2 put CSOs intermediate between other AGN and star forming galaxies (Willett+2010).

Comparison sample of AGN is heterogeneous containing two RGs (Armus+2007, Weedman+2005).

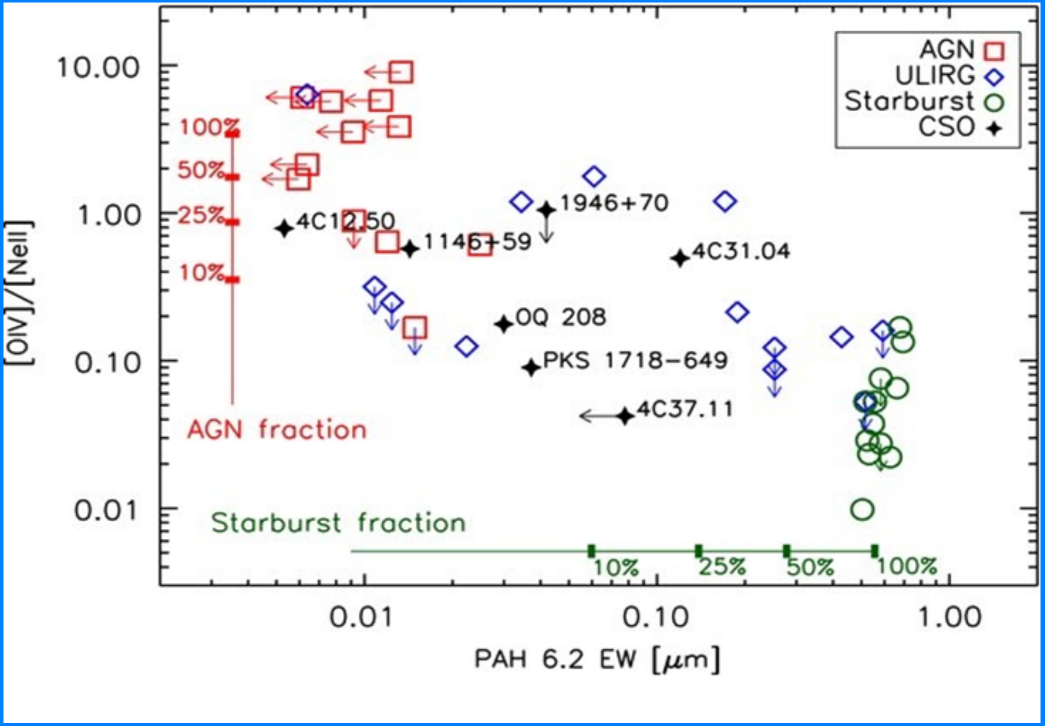

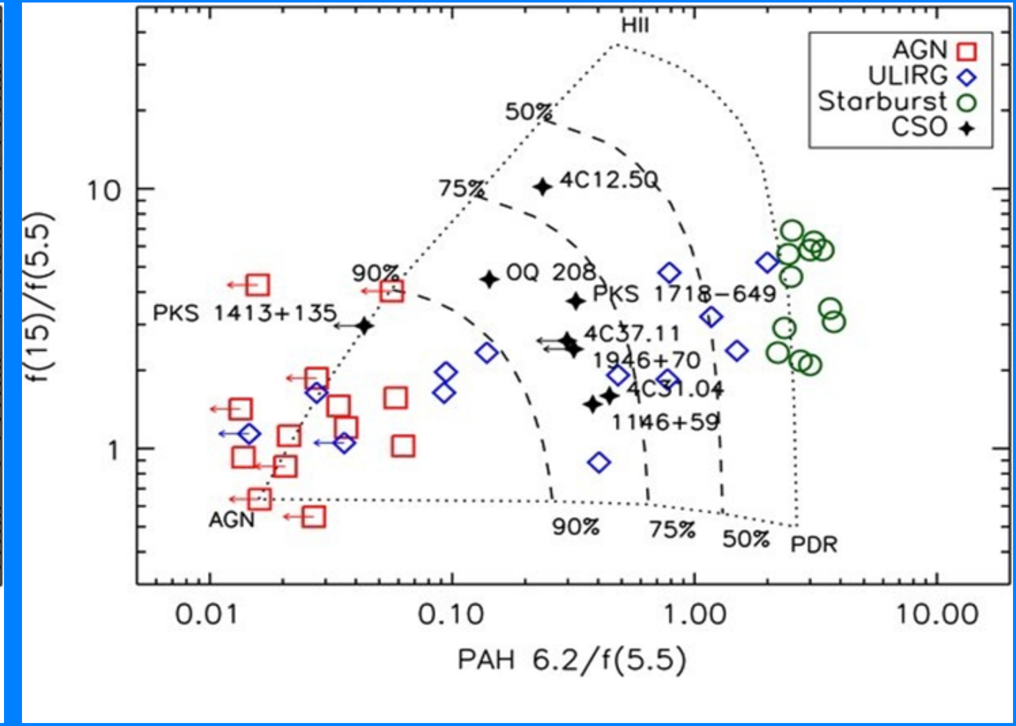

GPS/CSS Show Enhanced Star Formation

The 2Jy + 3CRR sample contains 1 GPS and 7 CSS sources (Dicken+2012)

1/1 GPS and 5/7 CSS show PAH 11.3 μm emission for 6/8 (75%) (Dicken+2012).

75% of GPS+CSS show (optical/mid-IR) evidence for recent star formation; while 21% of large radio galaxies show evidence for recent star formation (Tadhunter+2011, Dicken+2012).

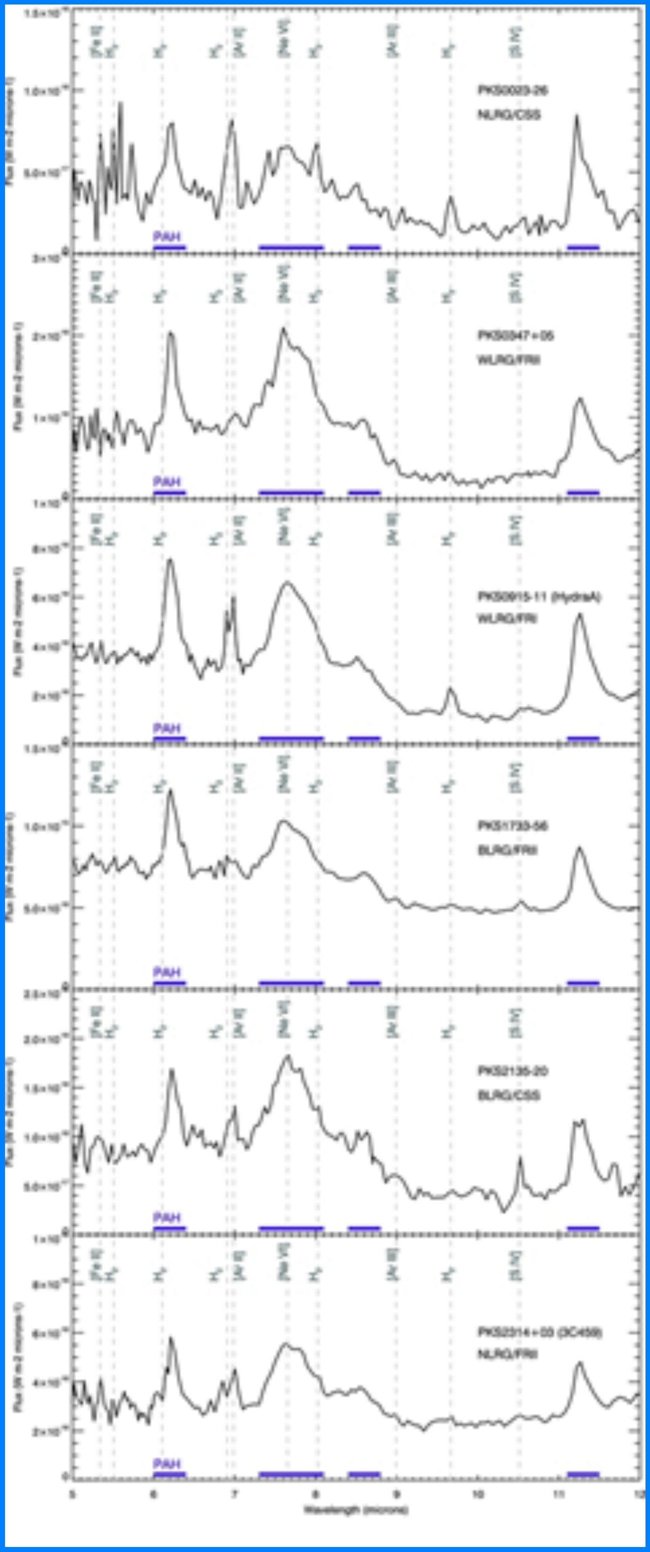

Magnified IRS spectra focusing on the 5–12 μm band of IRS to emphasize the dominant PAH bands at 6.2, 7.7, and 11.3 μm. The six objects in the 2 Jy sample with visually identifiable PAH emission are shown. Sample considered is 46 2 Jy radio galaxies ($0.05 < z < 0.7$) and 19 3CRR FRII radio galaxies ($z < 0.1$) (Dicken+2012).

GPS/CSS can have powerful central engines

Sample of 10 GPS (Stanghellini + 1998), 14 CSS (Fanti + 1995), and comparison sample of 25 large FRIIs (0.4 < z < 1.0) (Ogle+2015).

GPS and CSS have comparable mid-IR luminosity to large FRIIs. Much more luminous than Willett CSOs.

19/24 (79%) of GPS/CSS show high ionization lines ([Ne V] or [Ne VI])

Mid-IR luminosity at 15 and 7 μm vs. linear size. Q are *, RG are diamond. In 15μm plot, black crosses are CSOs from Willett+2010. Large FRII are red. (Ogle+2015)

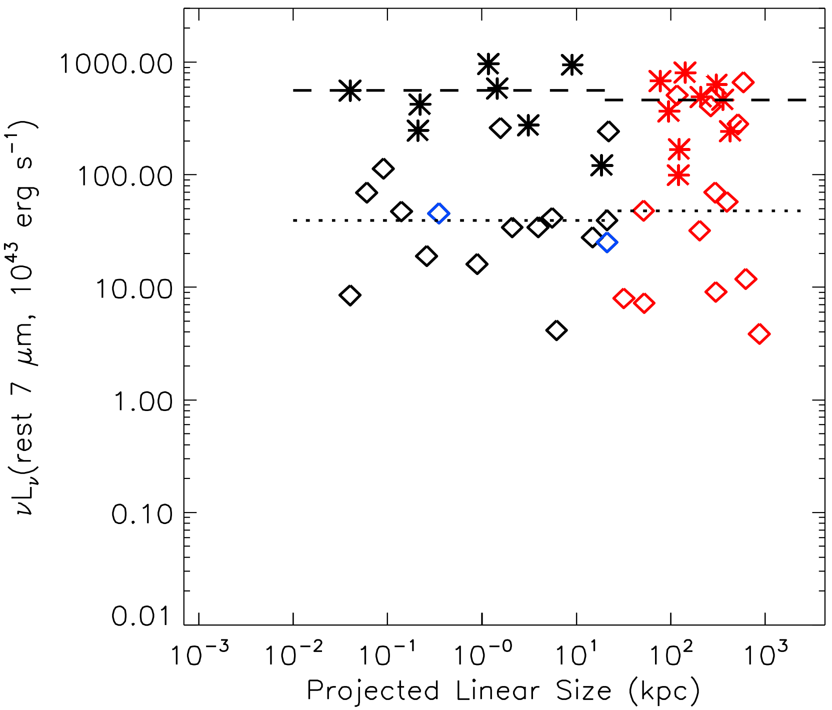

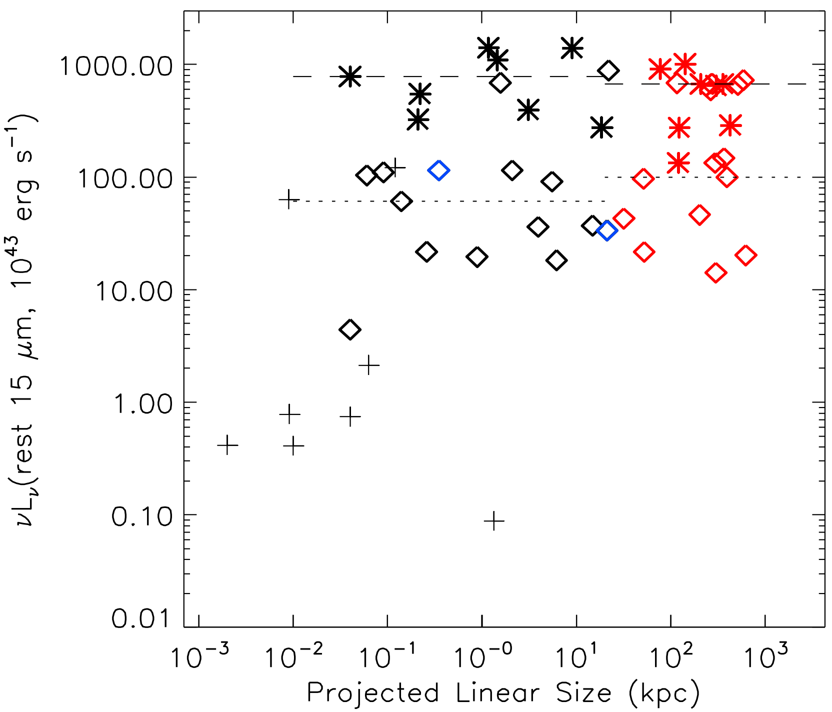

Evidence for High Star Formation not as Strong in Ogle Sample

4/24 (17%) GPS/CSS have detected PAH 7.7 µm emission and estimated SFR 10-60 M_o /yr. An additional 14/24 (58%) have upper limits on PAH which are consistent with this range of star formation (Ogle+2015)
So it's possible that this sample also has enhanced star formation.

Strong H_2 emission found in 5/24 (21%) of GPS/CSS consistent with strong jet-ISM interaction which shock heats the H_2 (Ogle +2015)

Number vs. Size

- Over the entire range N $\propto$ L $^{0.25}$
- There is a possible flattening at small size

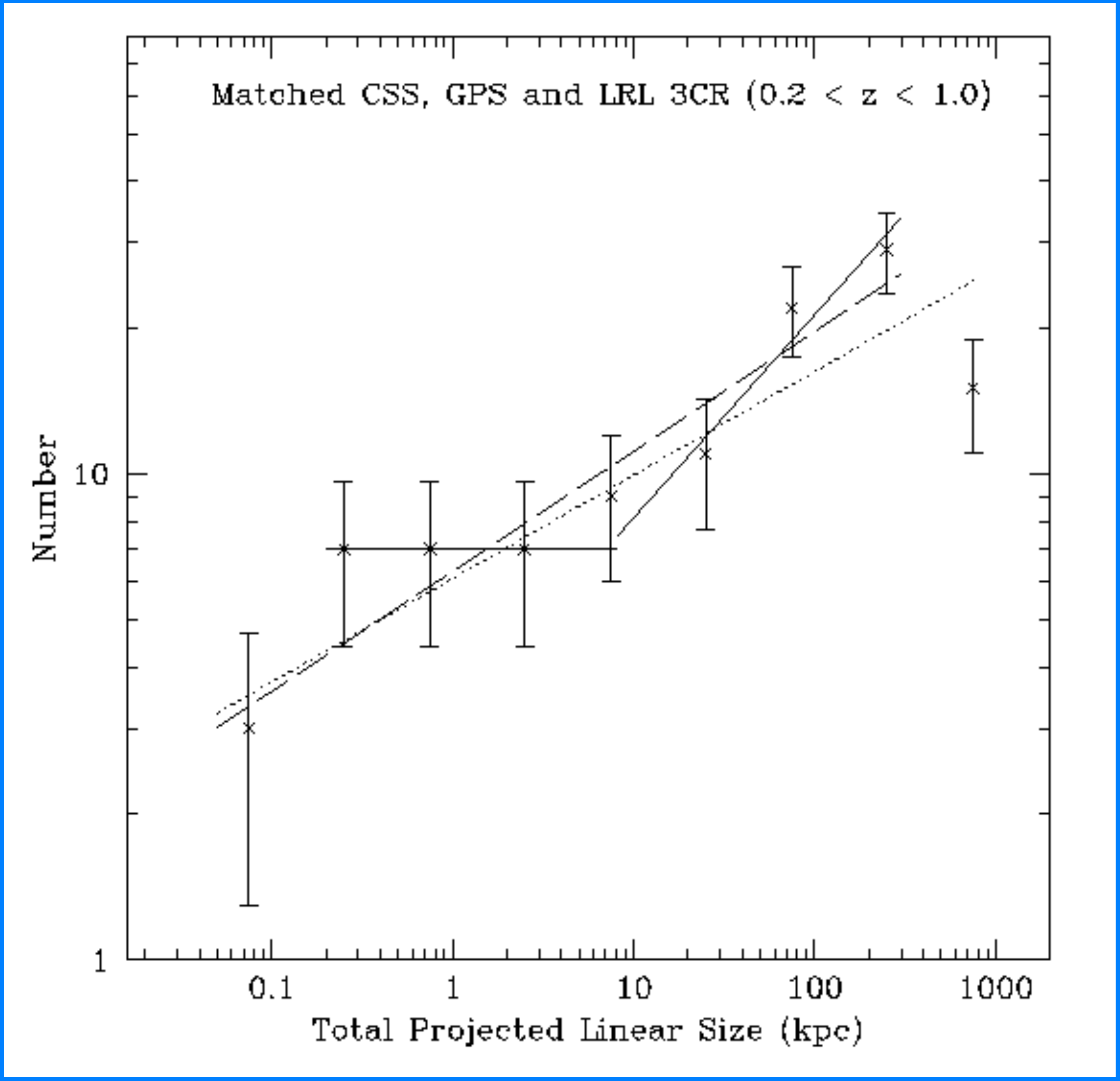

O'Dea (1998)

Multiple Episodes of Fueling?

- Numerical simulations of cold accretion:
- Delay in onset of AGN compared to onset of merger.
- Possible multiple episodes of cold gas fueling lasting about 10^8 yr.

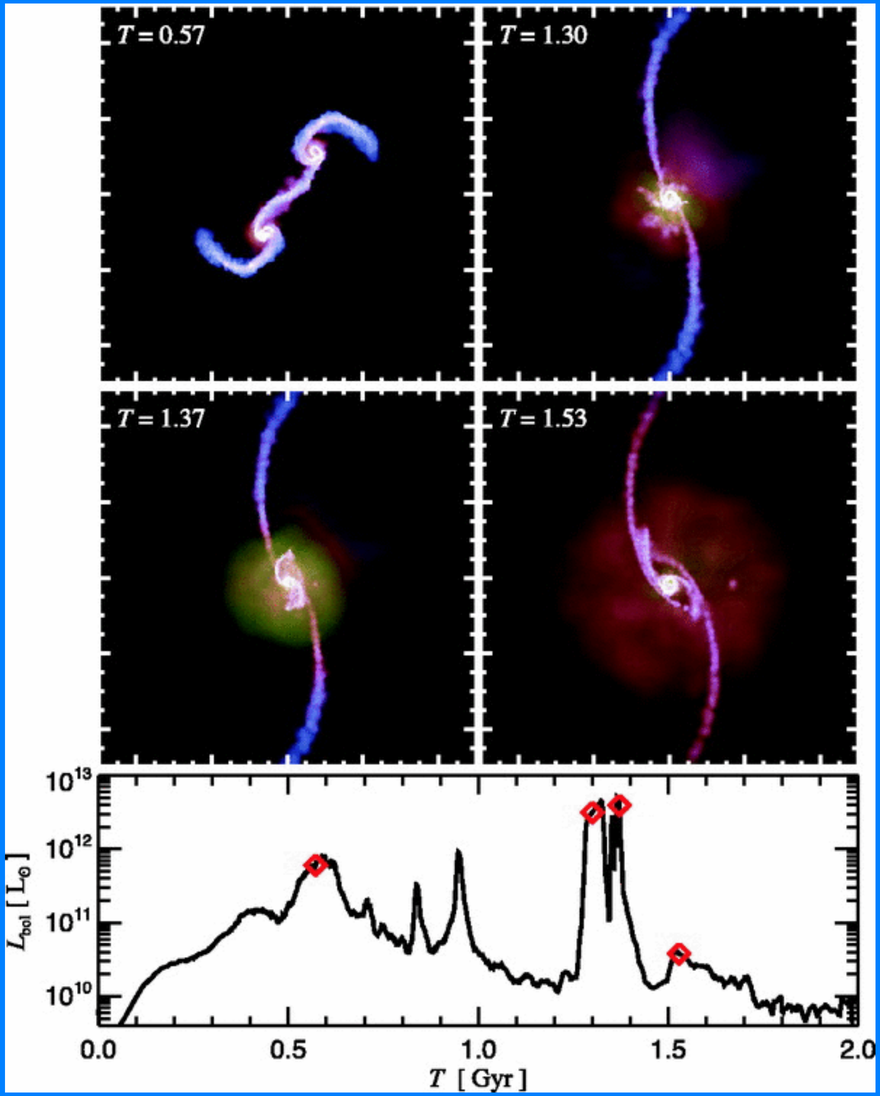

Projected gas density color coded by temperature (box 140 kpc across). Bolometric luminosity of central black hole(s), with diamonds marking the times shown above. (Hopkins+ 2005)

Implications. I

The IR confirms that some GPS/CSS can have central engines which are similar to those of the extended powerful radio sources. This is consistent with the hypothesis that some GPS/CSS can evolve to become the large scale sources.

The GPS/CSS seem to have higher star formation rates than typical (2JY + 3CRR) radio sources. Why?

1. GPS/CSS are triggered near the peak of star formation activity in a merger scenario.
2. Jet-induced star formation by GPS/CSS.
3. Radio power is enhanced by jet-ISM interaction in clumpy star-forming media (Tadhunter+2011, Dicken+2012).

But, Starburst Time-scales are Long

Hydro simulations of galaxy mergers suggest the starburst phase will have a lifetime of $\sim 10^8$ yrs. (di Matteo+ 2005).

A GPS triggered at the peak of a starburst (which is destined to evolve into a large RG) should do on time scales of $10^7 – 10^8$ yrs.

The large RG should still be associated with the starburst event. But most large RG are not found associated with a starburst event (Tadhunter+2011).

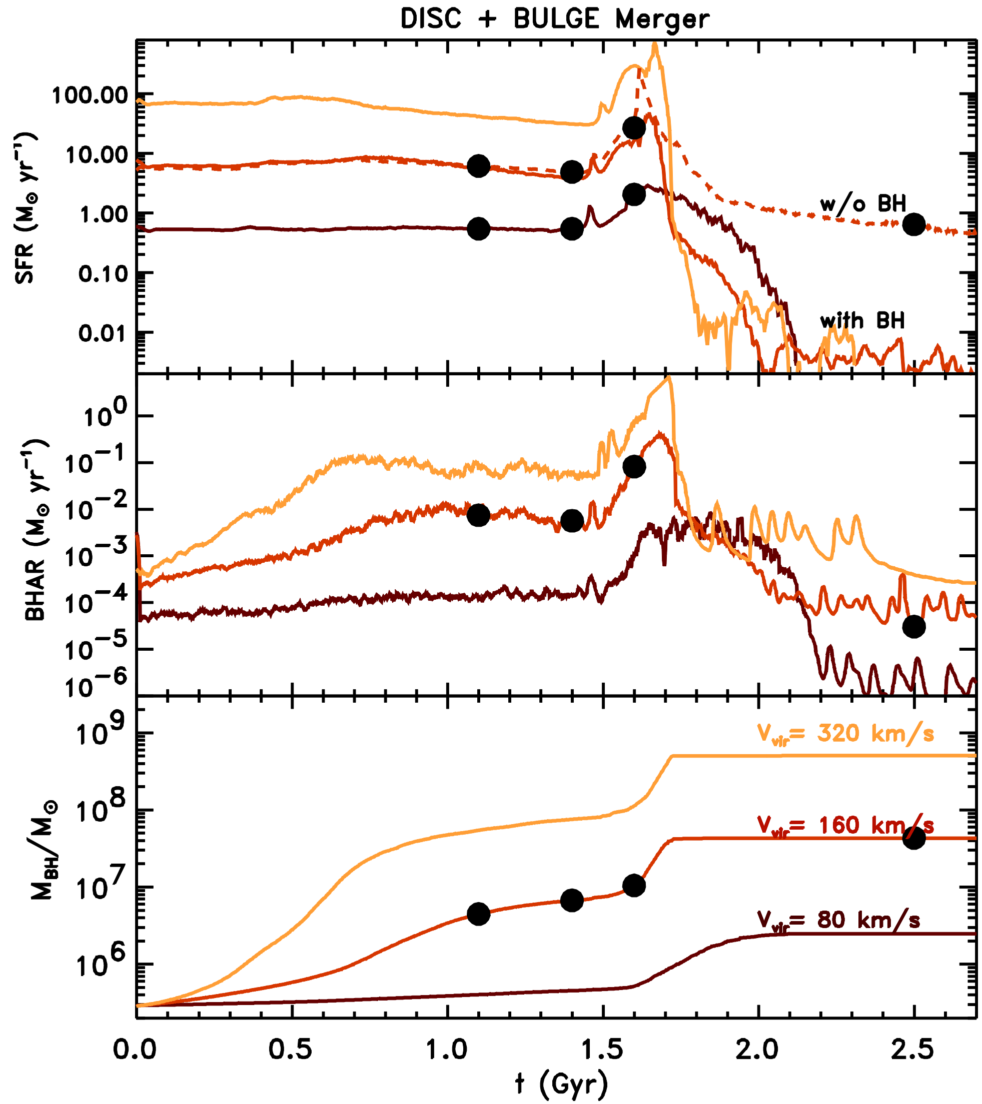

Black hole activity, star formation and black hole growth plotted as a function of time during a galaxy-galaxy merger. The star formation rate (SFR) and black hole accretion rate (BHAR) are given in units of solar masses per year. The black hole mass is given in units of solar masses. (di Matteo+2005).

Implications. I

The IR confirms that GPS/CSS can have central engines which are similar to those of the extended powerful radio sources. This is consistent with the hypothesis that the GPS/CSS can evolve to become the large scale sources.

The GPS/CSS seem to have higher star formation rates than typical (2JY + 3CRR) radio sources. Why? (see Tadhunter+2011, Dicken+2012).

Perhaps GPS/CSS are triggered near the peak of star formation activity. But because RG lifetimes are much less than starburst lifetimes, the large RGs should also be seen at the peak of star formation. But RGs are found at all stages of star formation activity (Tadhunter+2011).

UV Observations of Jet-Induced Star Formation?

- We find UV emission aligned with the radio source in 3C303.1. We suggest the emission is due to recent star formation which has been triggered by the expanding radio lobes.
- Probably not a lot of star formation.
- The lack of alignment in GPS sources suggests the UV emission is not scattered nuclear light.

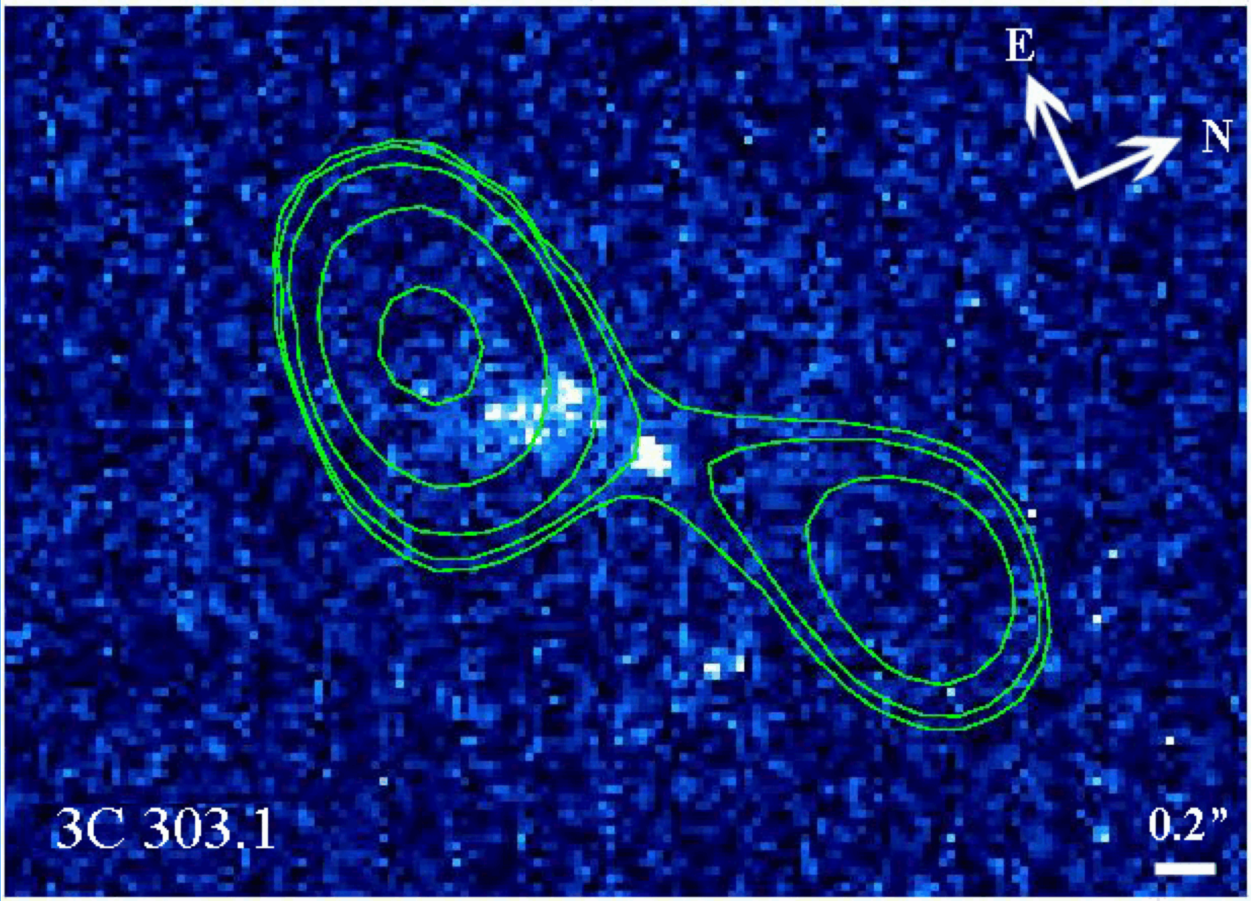

- Overlay of HST/ACS/HRC/F330W image on the radio source (green contours). The relative registration is uncertain, but the alignment between the radio and the UV is clear. (Labiano etal. 2008, A&A, 477, 491). Note image is rotated.

CSS Have Jet-Induced Star Formation?

•CSS exhibit the alignment effect in emission line gas (de Vries+ 1999, Axon+2000, Privon+2008).

•Evidence for jet induced star formation is still anecdotal. (Need more data!)

•3C303.1 shows UV emission aligned with radio source axis (Labiano+ 2008) associated with brightest lobe.

•Maybe these star formation events are impulsive? (no messy gas transport).

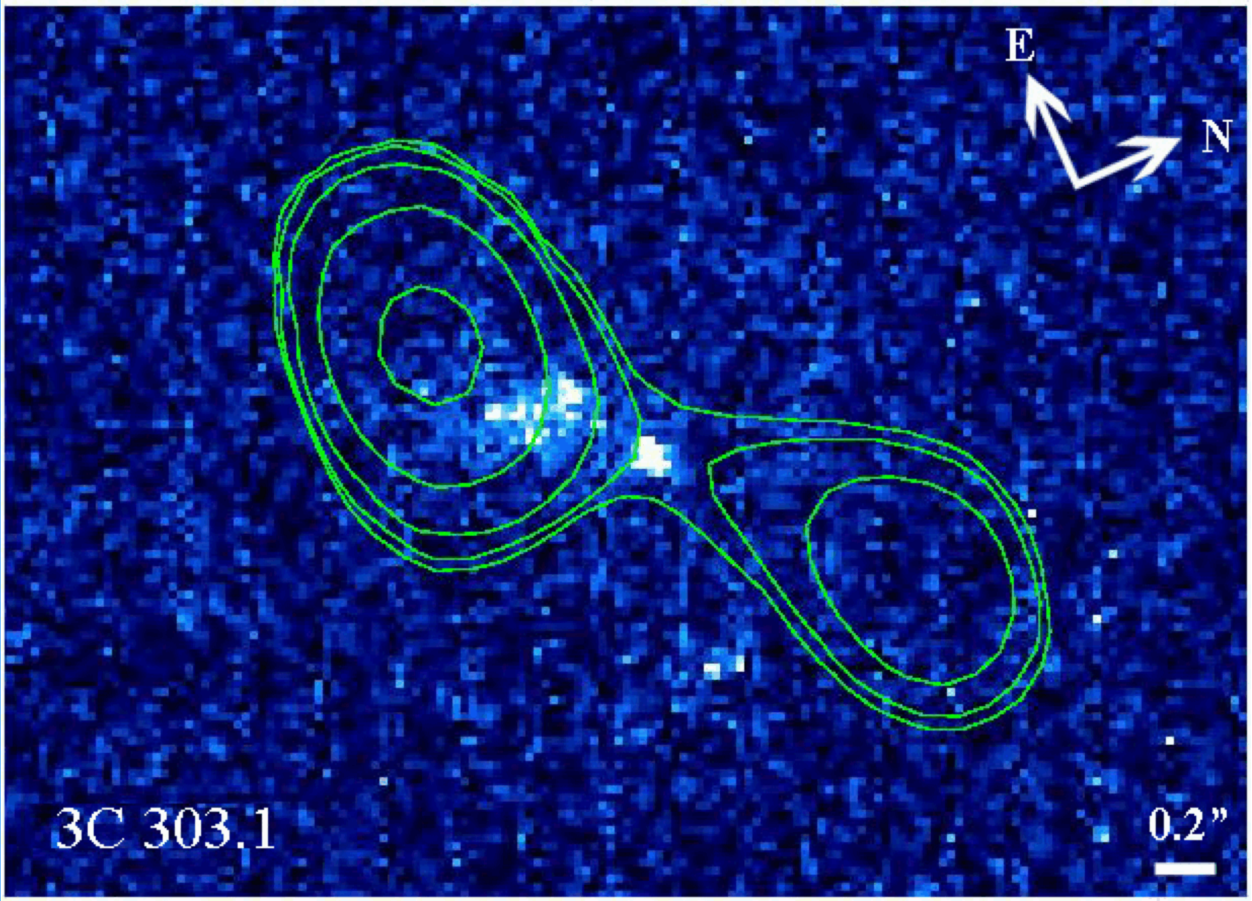

•Overlay of HST/ACS/HRC/F330W image on the radio source (green contours). The relative registration is uncertain, but the alignment between the radio and the UV is clear. (Labiano etal. 2008, A&A, 477, 491). Note image is rotated.

Asymmetries in "symmetric" objects

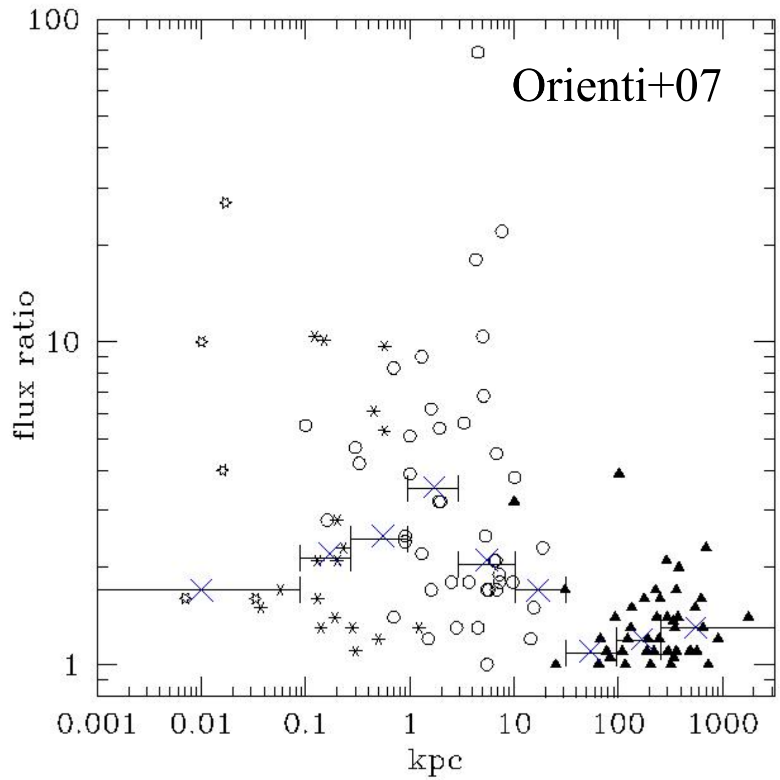

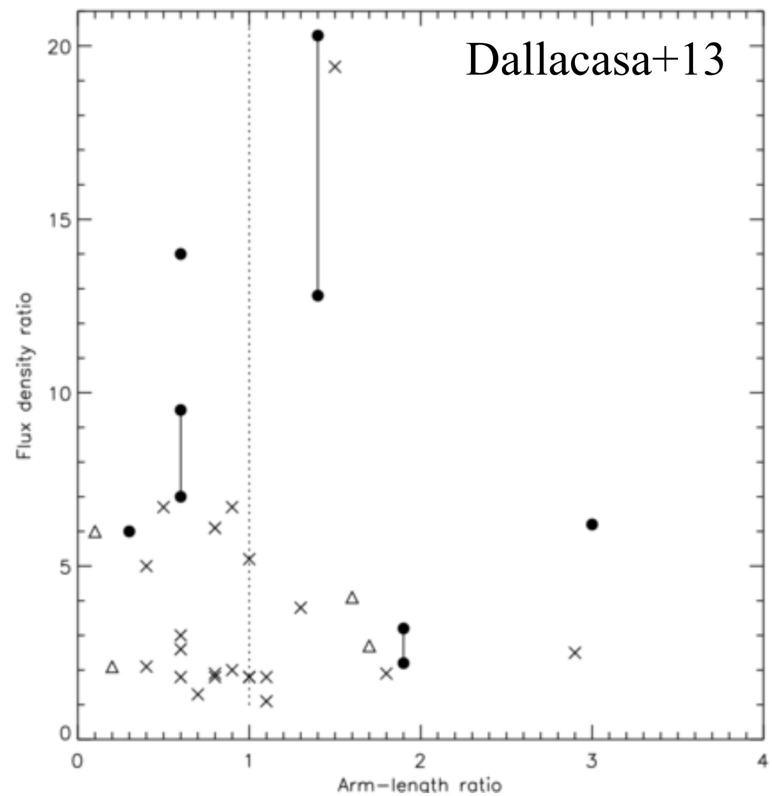

Large asymmetry in both luminosity and arm-length ratios between the lobes.

Saikia+ 03, Fanti+ 90, Dallacasa+13

Jet-ISM interaction?

Slide from M. Orienti

Implications. II

Assume that interactions of a compact radio source with dense, clumpy gas enhances radio emission (e.g., van Breugel+1985, Gopal-Krishna & Wiita 1991, Jeyakumar+2005). Brightness enhancements in interacting lobes ~ 2-10 (talk by Orienti).

Assume that the dense clumpy medium is also undergoing substantial star formation.

Then, GPS/CSS sources propagating through a dense, star forming medium will be preferentially selected in flux limited surveys because of the enhanced radio luminosity.

This will cause compact radio sources to be preferentially found in galaxies with significant star formation (e.g., Willett+2010, Tadhunter +2011, Dicken+2012, Ogle+2015).

This will also enhance the numbers of compact sources relative to larger sources (O'Dea & Baum 1997).

Excess of Sources at Small Size?

- Over the entire range N ~ L $^{0.25}$
- There is a possible flattening at small size (O'Dea & Baum 1997)
- Models which fit the data include
    - Intermittent sources (Reynolds & Begelman 1997)
    - A subpopulation which is disrupted on small scales (Alexander 2000)

(Top) data from the GPS, CSS, and LRL samples (O'Dea and Baum (1997, see also Fanti 2008) (Middle) Fit to the data which includes intermittent radio sources (Reynolds & Begelman 1997). (Bottom) Fit to the data which includes sources which disrupt on small scales (Alexander 2000).

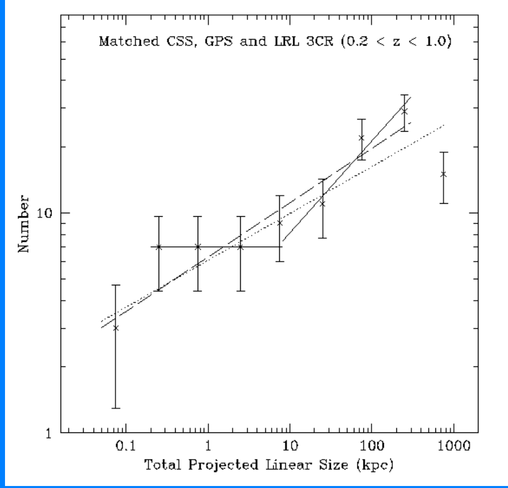

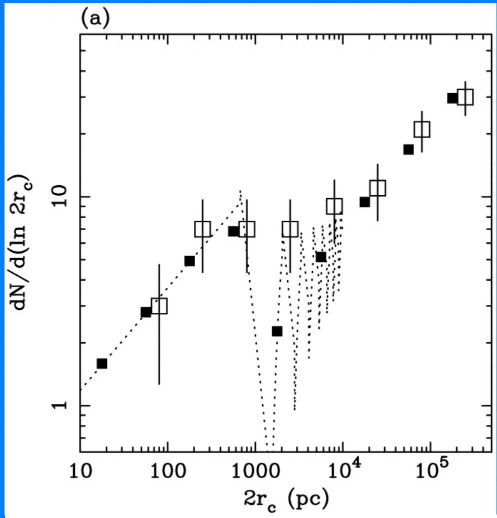

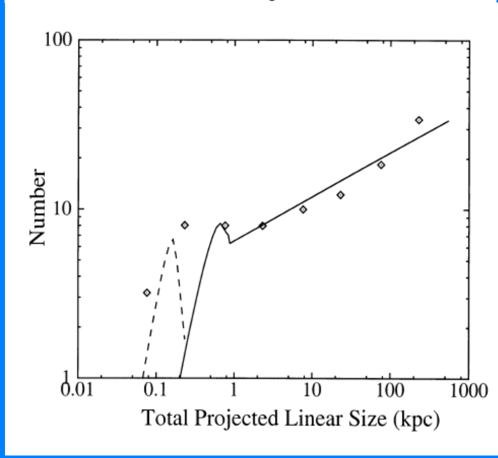

Dude, Where are my Progenitors?

If the presence of star formation means that the GPS/CSS are intrinsically low luminosity sources which cannot evolve into the powerful sources (e.g., 2Jy+3CRR). Then where are the sources which will evolve into the extended 2Jy+3CRR ?

Conclusion

Star formation seems like it could be more common in GPS/CSS that in larger sources.

This will provide important insights into the statistics of compact sources and their interactions with their environments.

We need more information on the properties and time scales of the star formation in compact sources.

Conclusions

Extra Slides

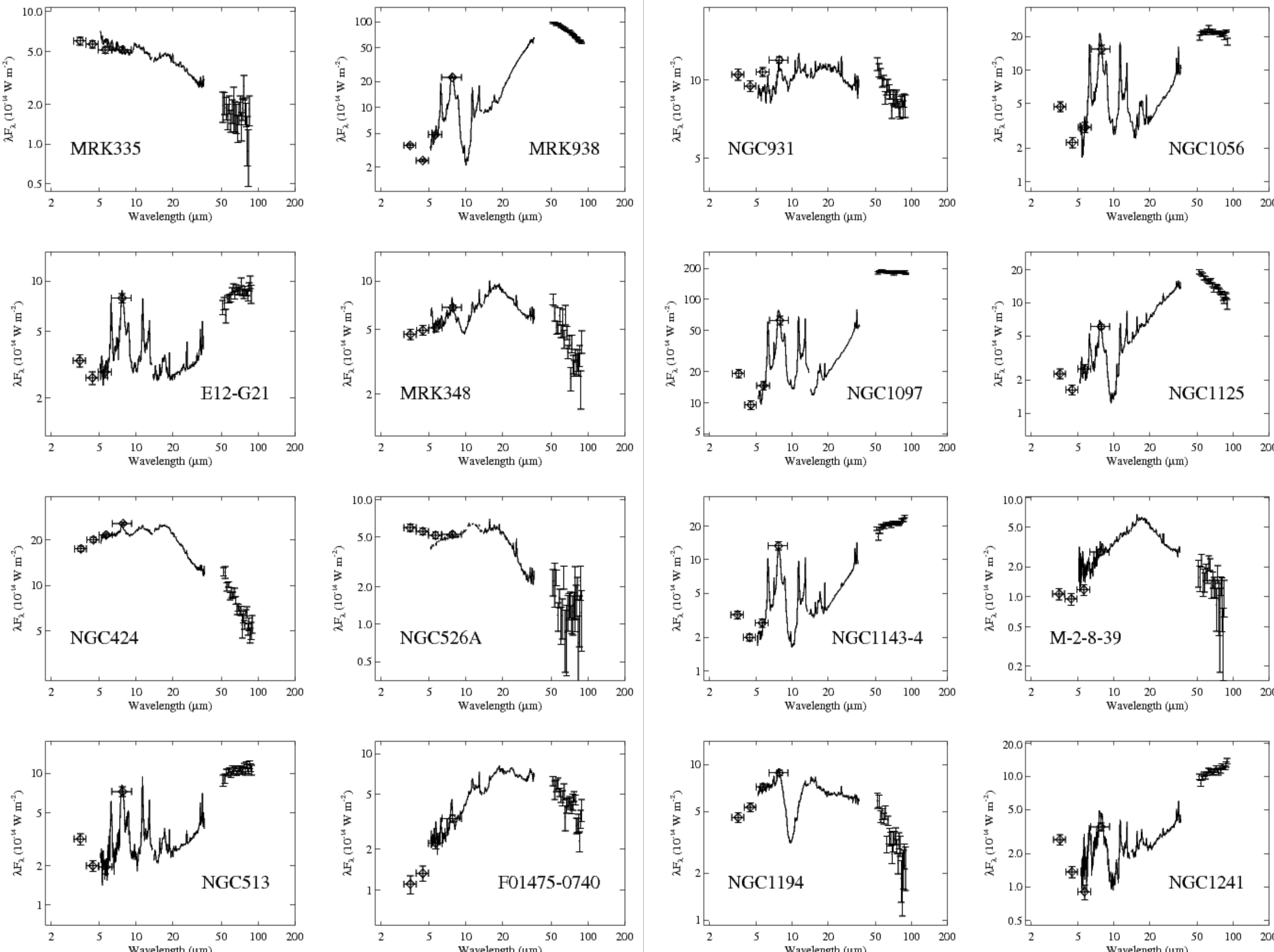
MRK335
MRK938
NGC931
NGC1056
E12-G21
MRK348
NGC1097
NGC1125
NGC424
NGC526A
NGC1143-4
M-2-8-39
NGC513
F01475-0740
NGC1194
NGC1241
λF_λ (10^-14 W m^-2)
Wavelength (μm)

[OIII]/[NeV] vs. SiI 9.7 µm

- Haas et al. (2005) showed that [OIII]λ5007 was orientation dependent in quasars and radio galaxies.
- We find that both [OIII]/[NeV] and [OIII]/[OIV] are rank correlated with SiI 9.7 µm strength, i.e., higher [OIII] λ5007 in face-on objects.
- This indicates that [OIII] λ5007 is orientation dependent in Seyferts. i.e., that much of the [OIII] emission is produced on scales which are at least partially obscured in the optical.

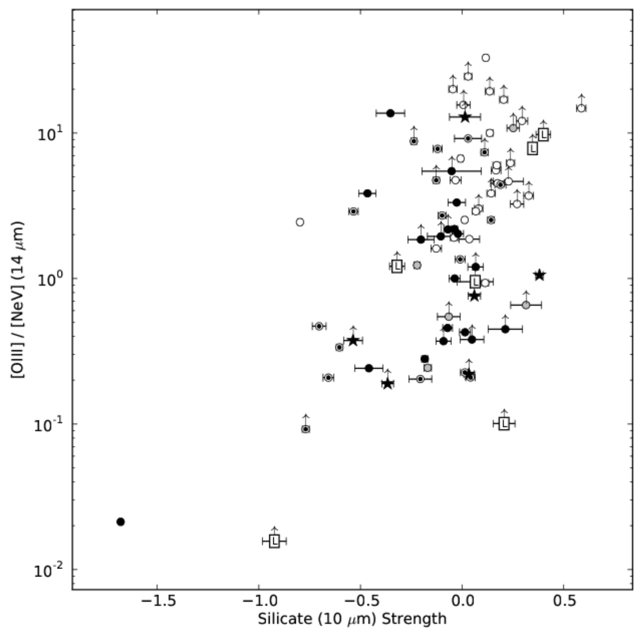

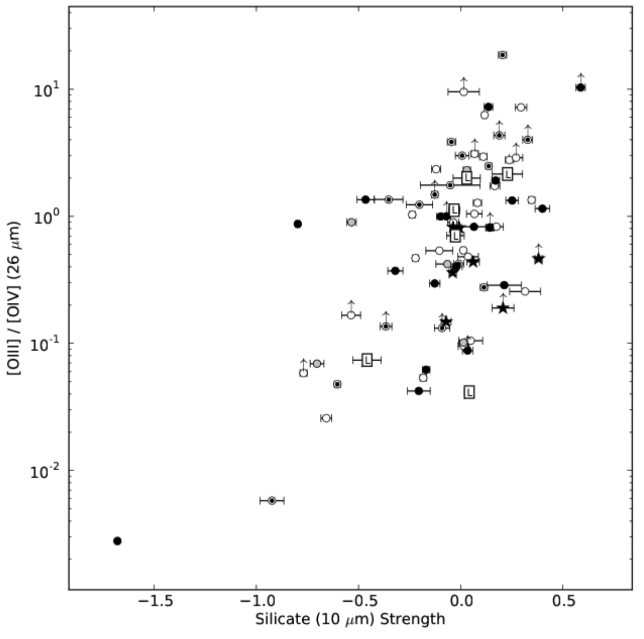

Sy 1-1.5: open circles, Sy 1.8,1.9 : gray-filled circles, Sy 2: filled circles, HBLR Sys (Sy 1h, and S1i): partially filled circles, LINERS: squares labled "L", Starburst/HII: stars. Limits are indicated by appropriately directed arrows. (Baum et al. 2010).